Monthly Notices
of the
ROYAL ASTRONOMICAL SOCIETY

MNRAS **469,** 4341–4358 (2017) doi:10.1093/mnras/stx1116

Photometric evolution of seven recent novae and the double-component characterizing the light curve of those emitting in gamma rays

U. Munari,[1]★ F.-J. Hambsch[2] and A. Frigo[2]

[1]*INAF Astronomical Observatory of Padova, I-36012 Asiago (VI), Italy*
[2]*ANS Collaboration, c/o Osservatorio Astronomico, via dell'Osservatorio 8, I-36012 Asiago (VI), Italy*

Accepted 2017 May 5. Received 2017 May 4; in original form 2017 March 27

ABSTRACT

The *BVI* light curves of seven recent novae (i.e. V1534 Sco, V1535 Sco, V2949 Oph, V3661 Oph, MASTER OT J010603.18–744715.8, TCP J1734475–240942 and ASASSN-16ma) have been extensively mapped with daily robotic observations from Atacama (Chile): five belong to the Galactic bulge, one to the Small Magellanic Cloud and another is a Galactic disc object. The two programme novae detected in γ-rays by Fermi-LAT (i.e. TCP J1734475–240942 and ASASSN-16ma) are bulge objects with unevolved companions. They distinguish themselves by showing a double-component optical light curve. The first component to develop is the fireball from freely expanding, ballistic-launched ejecta, with a time of passage through maximum that is strongly dependent on wavelength ($\sim$1 d delay between the *B* and *I* bands). The second component, emerging simultaneously with the nova detection in γ-rays, evolves at a slower pace, its optical brightness being proportional to the γ-ray flux, and its passage through maximum not dependent on wavelength. The fact that γ-rays are detected at a flux level that differs by four times from novae at the distance of the bulge seems to suggest that γ-ray emission is not a widespread property of normal novae. We discuss the advantages offered by high-quality photometric observations collected with only one telescope (as opposed to data provided by a number of different instruments). We also observe the effects of the wavelength dependence of fireball expansion, the recombination in the flashed wind of a giant companion, the subtle presence of hiccups and plateaus, and the super-soft X-ray emission and its switch-off. Four programme novae (V2949 Oph, V3661 Oph, TCP J18102829–2729590 and ASASSN-16ma) have normal dwarf companions: V1534 Sco contains an M3 III giant, V1535 Sco a K-type giant and MASTER OT J010603.18–744715.8 a subgiant. We also comment briefly on the maximum absolute magnitude relation with decline time (MMRD).

Key words: novae, cataclysmic variables.

1 INTRODUCTION

The outburst of a nova originates from thermonuclear runaway on the surface of a white dwarf (WD) when material accreted from a companion reaches critical conditions for ignition. The accreted envelope is electron-degenerate, a fact that leads to violent mass ejection into surrounding emptiness (if the donor is a dwarf) or into thick circumstellar material (if the WD orbits within the wind of a cool giant companion). The variety of nova phenomena is further enriched by the dependence on WD mass (as the velocity and amount of ejected material), the diffusion and mixing of underlying WD material into the accreted envelope (outburst strength and chemistry), the common-envelope interaction with the companion star, such as the three-dimensional (3D) morphology of the ejecta and duration of the post-thermonuclear stable nuclear burning, and the viewing angle (especially for highly structured ejecta composed of bipolar flows, equatorial tori, diffuse prolate components and winds or bow-shocks). Recently, Bode & Evans (2012), Saikia & Anupama (2012) and Woudt & Ribeiro (2014) have provided extensive reviews about classical novae.

Given the range of observable phenomena, a comprehensive description of a nova would obviously benefit from the widest wavelength and epoch coverage, including the pre-outburst properties of the progenitor. While there have been extensive studies of , for example, X-ray imaging/spectra (e.g. Ness 2012), GeV γ-ray detection (Ackermann et al. 2014) and radio high angular-resolution maps (Chomiuk et al. 2014), which are changing our understanding of novae, good multiband light curves are still an essential contribution to the field. In particular, during the initial optically thick phase, and also during the following optically thin advanced decline, the ejecta and pre-existing circumstellar matter reprocess at

★ E-mail: ulisse.munari@oapd.inaf.it

Table 1. The programme novae.

Name	RA	Dec.	*l* (Gal.)	*b* (Gal.)	Type	Discovery announced
V1534 Sco (Nova Sco 2014)	$17^h15^m46^s.83$	$-31°28'30''.3$	354.33	+03.99	He/N	2014 Mar 27.8
V1535 Sco (Nova Sco 2015)	$17^h03^m26^s.176$	$-35°04'17''.82$	349.90	+03.94	He/N	2015 Feb 13.8
V2949 Oph (Nova Oph 2015 N.2)	$17^h34^m47^s.75$	$-24°09'04''.2$	002.78	+04.59	Fe II	2015 Oct 14
V3661 Oph (Nova Oph 2016)	$17^h35^m50^s.50$	$-29°34'24''.0$	358.35	+01.48	Fe II	2016 Mar 11.9
MASTER OT J010603.18–744715.8	$01^h06^m03^s.18$	$-74°47'15''.8$	301.64	− 42.30	He/N	2016 Oct 14.3
TCP J18102829−2729590	$18^h10^m28^s.29$	$-27°29'59''.0$	003.99	− 04.04	Fe II	2016 Oct 20.4
ASASSN-16ma	$18^h20^m52^s.25$	$-28°22'12''.1$	004.33	− 06.48	Fe II	2016 Oct 26.1

longer wavelengths (optical/infrared) the energetic input of phenomena developing primarily at much higher energies. An accurate and multiband light curve of a nova can thus track and reveal a lot about the powering engine and the physical conditions in the intervening and reprocessing medium. In order to be of the highest diagnostic value, a multiband light curve should have the following properties:

(i) it should be densely mapped (daily);
(ii) it should start immediately after nova discovery and extend well into the advanced decline, stopped only by a solar conjunction or limited by telescope diameter;
(iii) it should pursue the highest external photometric accuracy (i.e. the combination of the highest recorded flux with the most accurate transformation from the instantaneous local photometric system to the standard one);
(iv) the entire (or the bulk of the) light curve should be obtained with a single instrument and it should not be the result of the combination of sparse data from a variety of different telescopes.

The last point is discussed in more detail in Section 3.

The aim of the present paper is to present extensive *BVI* light curves of seven recent novae, all appearing at deep southern declinations, well below those accessible with the Asiago telescopes that we regularly use spectroscopically to follow novae appearing north of $-25°$. The photometric observations presented in this paper have been obtained with a robotic telescope that we operate in Atacama (Chile). The programme novae are listed in Table 1, together with their equatorial and Galactic coordinates, spectral class (Fe II or He/N) and the date when their discovery was announced. All of them, except MASTER OT J010603.18–744715.8, which appears towards the Small Magellanic Cloud (SMC), erupted within a few degrees of the Galactic Centre.

Most of the programme novae have been targeted and detected in radio, X-rays and/or γ-rays. Nothing comprehensive has yet been published on these exciting observations other than preliminary announcements on ATels (e.g. a report on the radio and X-ray observations of V1535 Sco has just been submitted by Linford et al. 2017). There has only been a comprehensive study of the near-infrared (near-IR) spectra of the two oldest programme novae, V1534 Sco and V1535 Sco (Joshi et al. 2015; Srivastava et al. 2015b). No detailed reports on the optical properties and multiband light curves of the programme novae have been published so far. Thus, in this paper, our aim is to fill this gap by providing and discussing high-accuracy, daily mapped *BVI* light curves for all of the programme novae. In addition, to allow by themselves some physical discussion on the properties of the programme novae, our light curves are meant to provide useful supporting information for future studies based on other wavelength domains. Our photometric mapping started within one day of the nova announcement and extended until solar conjunction set in or the nova completed its evolution.

All times given in the paper are UT unless otherwise noted. Our photometry is strictly tied to the Landolt (2009) system of equatorial standards, thus the *I* band should be properly written as I_C (the Cousins system). For simplicity, we will drop the subscript 'C' in the rest of the paper, and write the adopted photometric bands as *BVI*.

2 OBSERVATIONS

BVI optical photometry of the programme novae was obtained with the Asiago Novae and Symbiotic Stars (ANS) Collaboration's robotic telescope 210, located in San Pedro de Atacama, Chile. All novae were observed ∼daily for as long as solar conjunction allowed after their discovery. Telescope 210 is a 40-cm *f*/6.8 Optimized Dall-Kirkham (ODK). It mounts an FLI-cooled CCD camera equipped with a 4k×4k Kodak 16803 sensor of 9-μm pixel size. The photometric *BVI* filters are of the multilayer dielectric type and are manufactured by Astrodon.

Technical details and operational procedures of the ANS Collaboration's network of telescopes are presented by Munari et al. (2012). Munari & Moretti (2012) have presented a detailed analysis of the photometric performances and multi-epoch measurements of the actual transmission profiles for all the photometric filter sets in use at all ANS telescopes. Data collected on the programme novae with ANS telescope 210 were transferred via ftp daily to the central ANS server where data reduction was carried out in real time to check on nova progress and instrument performance. Data reduction involved all the usual corrections for bias/dark/flat/pixel map, with fresh new calibration frames obtained regularly in spite of the highly stable conditions of the instrumentation at the remote desert site. Transformation from the instantaneous local photometric system to the standard one is carried out on all individual observations by colour equations whose coefficients are χ^2 calibrated against a local photometric sequence imaged together with the nova.

The local photometric sequence is extracted from the AAVSO Photometric All-Sky Survey (APASS; Henden et al. 2012; Henden & Munari 2014) using the transformation equation calibrated in Munari et al. (2014a,b). The APASS is strictly linked to the Landolt (2009) and Smith et al. (2002) systems of equatorial standards. The local photometric sequences around the programme novae are selected to fully cover the whole range of colours spanned by each individual nova and are kept fixed during the whole observing campaign, so as to ensure the highest (internal) consistency. Re-observing the local photometric sequences along with the respecting novae has allowed us to refine their magnitudes to extreme precision (well beyond the original APASS), including pruning from

Table 2. Our BVI_C photometry of the programme novae. This table is published in its entirety in electronic form only (see the supporting information). A portion is shown here for guidance regarding its form and content. Colours are given explicitly because, during data reduction, these are obtained independent of the magnitudes and are not computed from each other. The given uncertainties are the total error budgets, adding quadratically the Poissonian contribution on the nova to the uncertainty in the transformation from the instantaneous local photometric system to the standard one.

Nova	HJD (−245000)	Date (UT)	B	Err	V	Err	I	Err	$B-V$	Err	$V-I$	Err
V1534 Sco	6744.91970	2014-03-28.420	12.919	0.013	11.900	0.009	9.923	0.009	0.999	0.013	1.983	0.010
V1534 Sco	6745.91697	2014-03-29.417	13.101	0.026	12.121	0.012	10.230	0.014	0.942	0.027	1.932	0.018
V1534 Sco	6746.95239	2014-03-30.452	13.260	0.010	12.290	0.012	10.397	0.017	0.938	0.009	1.952	0.017
V1534 Sco	6747.63243	2014-03-31.132	13.600	0.016	12.558	0.009	10.490	0.007	1.043	0.016	2.100	0.013
V3661 Oph	7461.82492	2016-03-14.325	14.016	0.011	11.325	0.006	8.283	0.016	2.642	0.011	3.115	0.017
V3661 Oph	7461.89726	2016-03-14.397	14.004	0.010	11.345	0.005	8.227	0.012	2.619	0.009	3.167	0.012
V3661 Oph	7462.77606	2016-03-15.276	14.431	0.008	11.805	0.005	8.461	0.012	2.539	0.008	3.438	0.012
V3661 Oph	7462.82403	2016-03-15.324	14.397	0.007	11.822	0.005	8.403	0.011	2.499	0.007	3.441	0.010
V3661 Oph	7463.77358	2016-03-16.274	14.935	0.013	12.486	0.007	8.930	0.013	2.364	0.013	3.685	0.013
V3661 Oph	7463.82160	2016-03-16.322	14.963	0.011	12.486	0.006	8.851	0.012	2.369	0.011	3.641	0.014
⋮	⋮	⋮	⋮	⋮	⋮	⋮	⋮	⋮	⋮	⋮	⋮	⋮

the hidden presence of subtle variable stars. These pruned and refined local photometric sequences are freely available (e-mail the first author) to anyone interested in using them to calibrate further optical photometry of the novae considered in this paper.

All measurements were carried out with aperture photometry, with the aperture radius and inner/outer radii for the sky annulus χ^2-optimized on each image so as to minimize dispersion of the stars of the local photometric sequences around the transformation equations from the local instantaneous to the standard system. On average, the aperture radius was $\sim$1.0 $\times$ FWHM of the seeing profile, and the inner and outer radii for the sky annulus were $\sim$3 $\times$ and $\sim$5 $\times$ FWHM, respectively. Finally, colours and magnitudes are obtained separately during the reduction process, and are not derived from each other. Our measurements for the programme novae are listed in Table 2, available in full only electronically (see the supporting information). The quoted uncertainties are total error budgets, adding quadratically the Poissonian contribution on the nova to the uncertainty (measured on the stars of the local photometric sequence) in the transformation from the instantaneous local photometric system to the standard one.

3 SINGLE-TELESCOPE VERSUS MULTI-TELESCOPE LIGHTCURVES

The advantages offered by building the light curve of a nova from data provided by a single telescope (and thus not the result of the combination of sparse data from a variety of different telescopes) are relevant, even if frequently overlooked or not fully appreciated. Although they are themselves very relevant, we do not refer to differences in the quality of data acquisition/reduction/calibration carried out at each telescope, nor do we refer to the effect of difference in focal length and PSF purity in the crowded fields where novae usually appear. Here, we only consider the ideal case in which all aspects of data acquisition and reduction have been carried out using state-of-the-art photometry, and crowding is not an issue.

The spectral energy distribution (SED) of a nova is dominated by strong emission lines, the more so as the nova declines. While standard colour-equations (for either the all-sky or the local photometric sequence approaches) can essentially null the differences (for normal stars and standard filter sets) between the standard photometric system and its local instantaneous realization (with the time- and λ-dependent atmospheric transmission as a key component of the optical train), this is hardly so for objects whose spectra are dominated by emission lines.

Let us consider the Landolt V band, for example, with similar reasoning applicable to other bands or other photometric systems. As discussed in detail in Munari et al. (2013), much of the flux through the V band during the optically thin phase of Fe II novae comes from the [O III] nebular doublet. The doublet is located on the steeply rising long-pass edge of the V-band profile, where small differences in the transmission of the photometric filters cause large deviations in the flux collected from the nova. Similarly, during the optically thick phase of heavily reddened novae of both the Fe II and He/N types, a non-negligible fraction of the flux through the V band comes from the Hα emission line. Hα is located at the red wing of the V band, where the transmission of an actual filter can go from null up to several per cent of the peak value.

In the top panel of Fig. 1, we have plotted the transmission profile of the V band as locally realized by some of the most popular attempts to match and standardize the original Johnson & Morgan (1953) *UBV* photometric system (Cousins 1980; Graham 1982; Bessell 1990; Landolt 1992; Straižys 1992). The differences along the whole band profile are obvious. Yet, proper handling of the colour-equations can essentially null such differences when dealing with the smooth, continuum-dominated and blackbody-like SEDs of normal stars.

The lower three panels of Fig. 1 overplot the spectra of three novae with the transmission profiles of the set of V filters measured in the laboratory by Munari & Moretti (2012) with a spectrometer over the 2000 Å to 1.1 μm range (in order to check for either blue or red leaks). These filters come from the main manufacturers in the field and, prior to measurement, have been subject to at least one year of continuous operation at the telescope (thus exposed to large and continuous changes in barometric pressure, temperature and humidity). The filters are of two types. Those following the Bessell (1990) recipe for a sandwich of Schott coloured glasses (2 mm of GG495 + 3 mm of BG39) are plotted in orange; the others are of the multilayer dielectric type and are plotted in red. The nova spectra are examples taken from our long-term monitoring of all novae accessible with the Asiago telescopes. Nova Aql 2013 and Nova Oph 2009 are two heavily reddened novae, of Fe II and He/N types, respectively, as observed during the early decline from maximum.

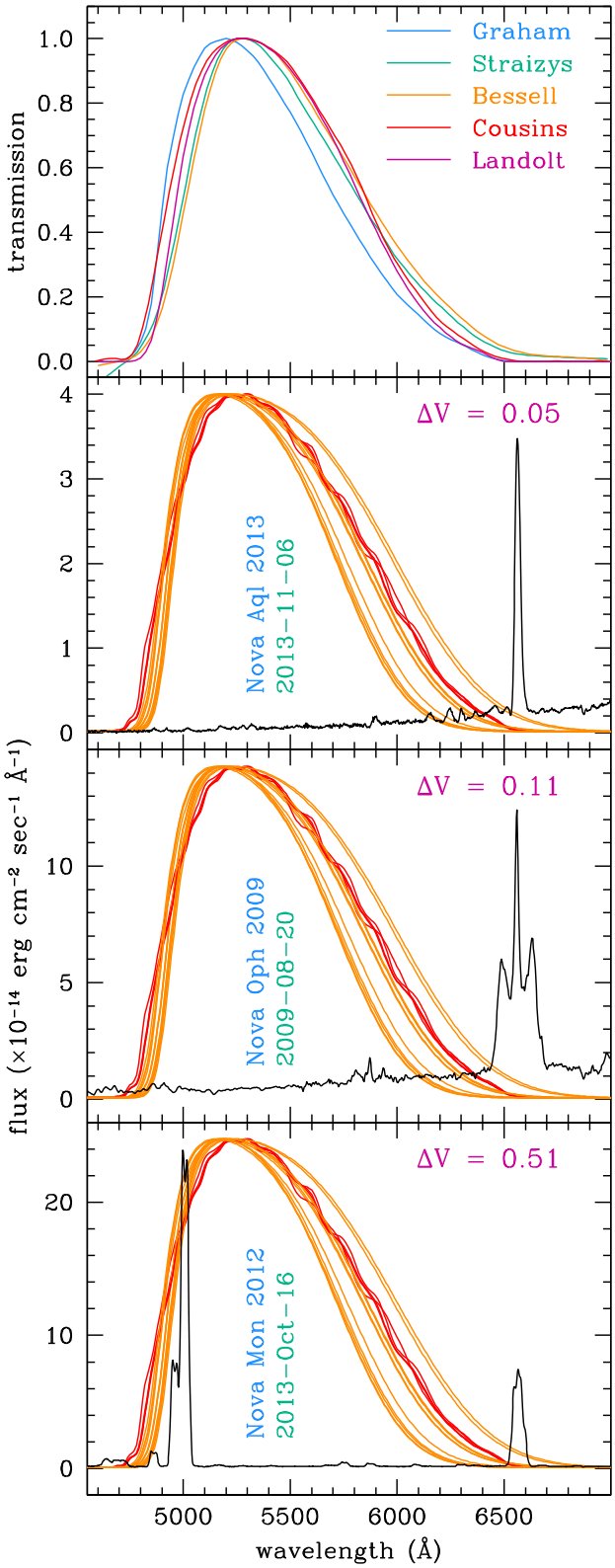

Figure 1. Top panel: natural *V* passbands for different realizations of the original Johnson's *V* band (see Section 3 for details). Lower three panels: examples of the ΔV shift that cannot be corrected by proper transformation to the standard photometric system for three types of nova spectra. The curves are actual transmission profiles for *V*-band filters from different manufacturers, as measured in the laboratory with a spectrometer by Munari & Moretti (2012). See Section 3 for details.

Nova Mon 2012 is a low reddening Fe II nova as observed during the optically thin phase, at a time when the super-soft phase was over.

To accurately simulate actual observations of these novae with the different *V* filters plotted in the lower panels of Fig. 1, we proceeded in the following way. The nights when these spectra of the three novae were observed were clear and all-sky photometric. Several blue and red spectrophotometric standard stars were observed at different airmasses during each night. On the fully extracted, but not flux-calibrated spectra of the standards, we computed the instrumental magnitude in the *UBV* filters, whose transmission profile is fully covered by our 3200–7700 Å spectra. These instrumental magnitudes (plus reference tabular values) were used with normal photometric data-reduction techniques to solve the colour-equations to transform from the local to the standard photometric system. While the *U*- and *B*-band profiles were kept fixed to those tabulated by Landolt (1992), for the *V*-band profile we in turn adopted each one of those plotted in the lower panels of Fig. 1.

The all-sky inter-calibration of the standard stars provided stable results at the 0.01-mag level in all bands whatever the choice for the *V* profile was. The *V* magnitude derived in the same way for the novae changed instead from one *V* filter to another. The range of the computed *V* magnitudes is (see Fig. 1) 0.05 mag for Nova Aql 2013, 0.11 mag for Nova Oph 2009 and 0.51 mag for Nova Mon 2012. For the heavily reddened Nova Aql 2013 and Nova Oph 2009, the bluer wavelengths going through the *V* passband contribute essentially nothing to the recorded flux. In such conditions, the fact that the transmission profile of a given filter is null, or is still transmitting something at the Hα wavelength, is the reason for the different magnitude derived for the nova. Obviously, the wider the equivalent width (EW) of Hα, the larger ΔV is, as the comparison of Nova Aql 2013 [EW(Hα) = 330 Å] and Nova Oph 2009 [EW(Hα) = 770 Å] clearly illustrates. For the nebular spectrum of Nova Mon 2012 (the lowest panel of Fig. 1), the line responsible for much of the filter-to-filter differences is [O III], which dominates [with its EW(Hα) = 8800 Å] the flux going through the *V* band. The [O III] doublet is located right on the steeply ascending branch of the *V*-band transmission profile, where filter-to-filter differences are the largest.

The conclusion seems straightforward. If state-of-the-art photometry is collected with only one telescope (always the same filters, detector, comparison sequence, data reduction procedures), any glitch present in a densely mapped light curve will probably be true (i.e. something connected to a real change in the physical conditions experienced by the nova). On the contrary, if the light curve of a nova is built from data obtained independently at different telescopes observing at different epochs, there is a serious risk that any feature is an artefact caused by the mixed data sources and that it is not intrinsic to the nova. In addition to those recorded by ANS Collaboration, excellent examples of single-telescope light curves of novae are those obtained by the SMARTS project (Walter et al. 2012) and the OGLE microlensing experiment (Mróz et al. 2015, 2016b).

Application of medium- and narrow-band filters to the photometry of novae would overcome the problems caused by the mixed presence of both continuum and emission lines within the transmission profile of broad photometric bands, segregating the contribution of pure continuum from that of emission lines. The evolution of Nova Del 2013 during the first 500 d of its eruption has been monitored by Munari et al. (2015) simultaneously in Landolt broad-band *B* and *V*, Stromgren medium-band *b* and *y*, and line narrow-band Hα and [O III] filters. This study highlights the great diagnostic potential of such a combined approach in carrying out the photometry of nova outbursts.

Table 3. Summary of some of the basic parameters for the programme novae as derived from our light curves. For TCP J18102829–2729590 and ASASSN-16ma, the values in square brackets are computed relative to the second maximum, the others to the first maximum. See sections on individual novae for further data and details.

Name	V1534 Sco Nova Sco 2014	V1535 Sco Nova Sco 2015	V2949 Oph Nova Oph 2015 N.2	V3661 Oph Nova Oph 2016	MASTER OT J010603.18–744715.8	TCP J18102829 −2729590	ASASSN-16ma
Date(max, V)	2014/3/28.0[a]	2015/2/14.3	2015/10/12.38	2016/03/12.75	2016/10/9.8	2016/10/24.60	2016/11/8.0
t(max, V)[b]	6744.5[a]	7067.8	7307.88	7460.25	7671.3	7686.1 [7693.5]	7700.5 [7707.5]
B(max)			13.13	13.21		8.36 [8.33]	6.25 [6.96]
V(max)	11.55	9.70	11.41	10.79	9.50	7.54 [7.61]	5.90 [6.51]
I(max)	9.85		9.90	8.06		6.69 [6.47]	5.59 [5.71]
$V(15)$[c]		11.89	13.49	15.56	12.25	8.88 [10.21]	8.99 [10.20]
$(B-V)_{\max}$		+0.86		+2.50		+0.82 [+0.61]	+0.41 [+0.51]
$(B-V)_{t2}$	+1.09[d]	+0.94		+2.35	−0.32	+0.40 [+0.41]	+0.31 [+0.38]
$(V-I)_{\max}$		+1.73	+1.51	+3.74		+0.84 [+1.23]	+0.12 [+0.74]
$(V-I)_{t2}$	+2.09	+1.66		+3.99	+1.23	+1.38 [+1.41]	+1.34 [+1.37]
$E(B-V)^{\max}$		1.09		2.27		0.59 [+0.38]	0.18 [0.28]
$E(B-V)^{t2}$	1.11[d]	0.96		2.37	0.08[e]	0.42 [+0.43]	0.33 [0.40]
A_V (Schlafly[f])	6.15	2.88	2.93	11.48	0.10	1.41	0.95
A_V (Schlegel[g])	7.36	3.39	3.53	13.25	0.12	1.64	1.09
t_2^V (d)	5.6	13.9		3.9	8.8	18.0 [11.0]	11.3 [6.5]
t_3^V (d)	9.2	21.1		5.7	17.4	23.5 [16.5]	14.5 [10.5]
M_V (t2)	−9.41	−8.40		−9.81	−8.91	−8.12 [−8.66]	−8.63 [−9.24]
M_V (t3)	−9.54	−8.63		−10.07	−8.84	−8.51 [−8.90]	−9.04 [−9.40]
M_V (S-shape)[h]	−9.48	−8.83		−9.58	−9.28	−8.39 [−9.22]	−9.19 [−9.58]
Dist (kpc)	7.4	9.7		3.7	44.8	7.0 [11.2]	6.4 [9.2]
Dist(15)[i] (kpc)		8.2	8.4	5.9	40.5	4.5 [9.8]	7.0 [10.7]
ΔI[j]	4.4	7.2	>7.3	>13.9	11.5[k]	>15.3	>16.4

[a] In the I band instead of V band.
[b] JD − 245 0000.
[c] V mag 15 d past optical maximum.
[d] Not to be trusted, being affected by blended field stars in an overcrowded field.
[e] Average $E(B-V)$ toward SMC (Mateo 1998).
[f] Total extinction along the line of sight from SF11.
[g] Total extinction along the line of sight from SFD98.
[h] The stretched S-shape curve introduced by Capaccioli et al. (1989).
[i] Distance derived from the observed V mag 15 d past optical maximum.
[j] Amplitude of the outburst in I band.
[k] In the V band instead of I band.

4 THE PROGRAMME NOVAE

4.1 Decline rates, reddening and distances

For all the programme novae, the collected *BVI* photometric data allow us to derive decline rates, reddening and distances with the popular methods summarized in this section. The results are listed in Table 3, and in the sections below for the individual objects. The uncertainties on the times of maximum are about ±0.1 d, and ±0.01 mag on the photometric quantities.

The characteristic rates t_2^V and t_3^V are the time (in d) that a nova takes to decline in the V band by 2 and 3 mag, respectively, below maximum brightness. This quantity is obviously wavelength-dependent, considering the significant colour evolution presented by a nova around maximum. Duerbeck (2008) proposed a mean relation $t_3^V = 1.75 \times t_2^V$. For our programme novae, we obtain $t_3^V = 1.54 \times t_2^V$ ($\sigma = 0.22$).

Photometric reddening is computed by comparison with the intrinsic colours given by van den Bergh & Younger (1987). From a sample of well-studied novae, they derived as mean intrinsic values $(B-V)_\circ = +0.23(\pm 0.06)$ at the time of V-band maximum, and $(B-V)_\circ = -0.02(\pm 0.04)$ at t_2^V. The reddening values we computed for the programme novae at these two epochs are in good mutual agreement. Because of the peculiar SED of novae, the intrinsic values given by van den Bergh & Younger cannot be ported to other colour combinations using transformations calibrated on normal stars, as discussed in Munari (2014).

The distance to a nova is usually estimated via calibrated relations – called the magnitude at maximum vs. rate of decline (MMRD) – between absolute magnitude at maximum and rate of decline t_n^λ, either in the form

$$M_{\max}^\lambda = \alpha_n \log t_n^\lambda + \beta_n,$$

or in the stretched S-shaped curve

$$M_{\max}^\lambda = \gamma_n - \delta_n \arctan \frac{\epsilon_n - \log t_n^\lambda}{\zeta_n},$$

first introduced by Capaccioli et al. (1989). In computing the distances to the programme novae, we have adopted the latest available calibration by Downes & Duerbeck (2000) for the MMRD as a function of t_2^V and t_3^V, as well as the S-shaped curve. These three

values for the absolute magnitude are in good mutual agreement (mean deviation from the mean value is 0.15 mag), with perhaps a slight tendency to be fainter for values computed from t_2^V. The distance given in Table 3 is computed from the mean value of the absolute magnitude as provided by the three t_2^V, t_3^V and S-curve methods.

Buscombe & de Vaucouleurs (1955) noted how the absolute magnitude 15 d after optical maximum is similar for novae of all speed classes. We adopt for this the value $M_{15}^V = -6.05$ calibrated by Downes & Duerbeck (2000). On average, the distance computed in Table 3 from the brightness at 15 d is similar to that provided by the t_2^V, t_3^V and S-curve methods.

In estimating the distances, the correction for extinction is computed from the derived $E(B-V)$ reddening and the standard $R_V = 3.1$ law by Fitzpatrick (1999), following the expression

$$A(V) = 3.26 \times E(B-V) + 0.033 \times E(B-V)^2, \quad (1)$$

computed by Fiorucci & Munari (2003) for the energy distribution of a nova at the time of maximum brightness. Compared to the total extinction along the line of sight provided by the 3D maps of Schlegel, Finkbeiner and Davis (1998, hereafter SFD98) and Schlafly & Finkbeiner (2011, hereafter SF11), the extinction computed from equation (1) is nearly identical for four programme novae, and a fraction of it for the other two. The remaining programme nova (V2949 Oph) has no *B*-band photometry useful to the computation of $E(B-V)$.

Before closing this section, a brief comment seems in order about the MMRD relation, whose existence has sometimes been questioned (e.g. Shara et al. 2017), based mainly on a report by Kasliwal et al. (2011, hereafter K11) who claimed the discovery of a new and rich class of fast and faint novae in M31. Such anomalous novae would have been well within the detection limit of photographic and CCD-based surveys, which, during the last half century, have been continuously looking for novae in M31. Yet, apparently none of these surveys seems to have detected them. For example, the deep POINT-AGAPE microlensing survey (Darnley et al. 2004, 2006) discovered 20 novae in M31, following the well-established MMRD relation. None of the 10 novae observed by K11 in M31 seems normal, all being underluminous. It would seem that some systematics has affected the K11 analysis. The light curves presented by K11 are generally noisy and scarcely sampled, frequently catching the nova while already declining and thus probably missing the true maximum. In addition, as shown by Munari (2014) in a comparison with well-observed Galactic novae, the unusual way chosen by K11 to estimate the extinction has probably introduced another strong systematic offset. For the past 16 yr, the OGLE microlensing survey has continuously monitored the Magellanic Clouds, where reddening is not an issue, discovering 20 novae and providing exquisite light curves for them all (Mróz et al. 2016b). No object of the type claimed by K11 seems to be present among them. Finally, the existence of an MMRD relation (independently from the analytical form used to express it) is proven by the ∼30 Galactic novae close enough to the Sun for their ejecta to be spatially resolved so that an expansion parallax can be computed on purely geometrical grounds, as done by Downes & Duerbeck (2000) in calibrating their MMRD expressions. The soundness of these distances (and thus of the inferred MMRD relation) has been recently confirmed on completely different grounds by Özdönmez et al. (2016), who compared the reddening affecting these spatially resolved Galactic novae with the reddening progression along the lines of sight to them.

4.2 V1534 Sco

V1534 Sco (= Nova Sco 2014 = TCP J17154683–3128303) was discovered at (unfiltered) 10.1 mag on 2014 Mar 26.85 by K. Nishiyama and F. Kabashima (CBET 3841). Spectroscopic classification as an He/N nova was obtained on Mar 27.8 by Ayani & Maeno (2014), reporting FWHM = 7000 km s^{-1} for Hα (see also Jelinek et al. 2014).

Joshi et al. (2015) discuss the result from near-IR spectroscopy covering the first 19 d of the outburst, following on from the preliminary report by Joshi et al. (2014). The near-IR spectra confirm the He/N classification, and show emission lines characterized by a rectangular shape with FWZI ∼ 9500 km s^{-1} and a narrow component on the top. The positional coincidence with a bright Two-Micron All-Sky Survey (2MASS) cool source ($J = 11.255$, $H = 10.049$, $K_s = 9.578$) and the presence of first overtone absorption bands of CO at 2.29 μm (as seen in M giants) led Joshi et al. (2014) to suggest that V1534 Sco is a nova originating from a symbiotic binary system, similar to V407 Cyg, RS Oph and V745 Sco.

X-ray emission from the nova was observed by the *Swift* satellite within a few hours of optical discovery (Kuulkers et al. 2014), corresponding to an absorbed optically thin emission of $kT = 6.4^{+3.8}_{-2.1}$ keV and $N_{\rm H} = 5.8(^{+1.2}_{-1.0})10^{22}$ cm^{-2} (with most of the absorption intrinsic to the source). X-ray emission was also recorded on the following days (Page, Osborne & Kuulkers 2014), with the softer counts increasing as a result of decreasing absorption column, a behaviour consistent with that expected for a shock emerging from the wind of the secondary star, as expected in a nova erupting within a symbiotic system.

However, the presence of a cool giant in the nova V1534 Sco does face some inconsistencies. (i) The sequence of Joshi et al. (2015) of near-IR spectra shows emission lines of constant width, not the rapid shrinking associated with the deceleration of the ejecta expanding through the pre-existing wind of the cool giant companion, as observed in the template V407 Cyg case (Munari et al. 2011). (ii) The narrow peak, observed by Joshi et al. (2015) to sit on top of the broad emission lines, and taken to represent the flash-ionized wind of the cool giant, does not quickly disappear as a consequence of rapid recombination driven by the high electronic density, as observed in other novae erupting within symbiotic binaries. (iii) By analogy with V407 Cyg and V745 Sco, γ-ray emission would have been expected to arise from high-velocity ejecta slamming on to the wind of the cool companion (Ackermann et al. 2014), but no γ-ray detection of V1534 Sco has been reported to date.

4.2.1 *The light curve*

The light curve of V1534 Sco is presented in Fig. 2 and the basic parameters extracted from it are listed in Table 3. Our photometric monitoring commenced within 1 d of the announcement of its discovery. Our observations continued for a longer period than shown in the figure, but we refrain from plotting or tabulating such noisy late data, which are best described as a rapid flattening of the light curve towards the asymptotic values $B \sim 19.6$, $V \sim 18.3$ and $I \sim 14.3$. This flattening is artificial and can be ascribed to (i) the stable contribution from the 2MASS cool source, which dominates in the *I* band, and (ii) the unresolved contribution in the *B* and *V* bands by several unrelated field stars that lie within ∼4 arcsec of the nova. The crowding is so severe in the immediate surroundings of the nova that attempts to disentangle it via PSF-fitting proved unconverging on our images.

The time and brightness of the maximum in the *I* band is well constrained in Fig. 2 and, by similarity, we assume that the earliest

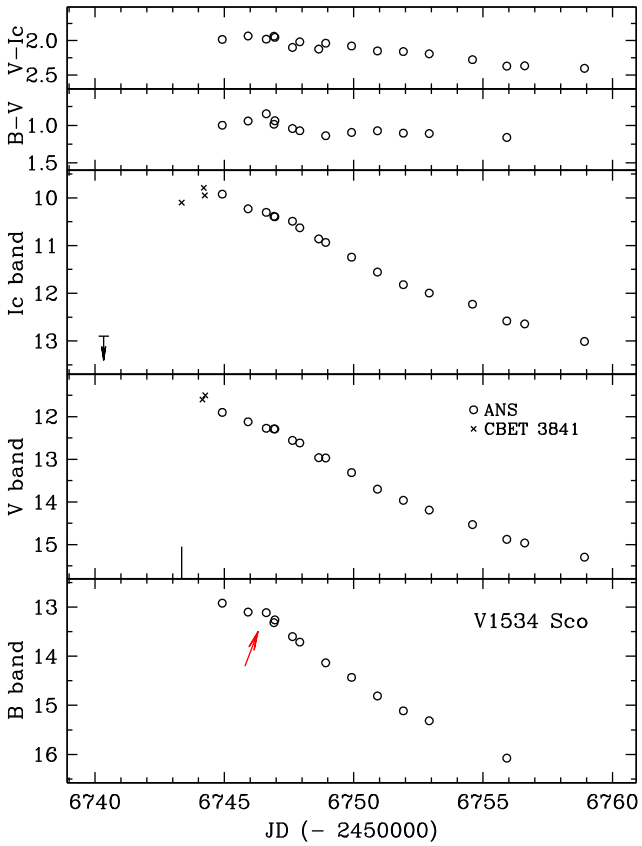

Figure 2. *BVI* photometric evolution of V1534 Sco (= Nova Sco 2014 = TCP J17154683–3128303). Data from CBET 3841 are reported as crosses and upper limit. The solid vertical line in the *V*-band panel marks the time of nova discovery. The arrow points to the hiccup considered in Fig. 3.

two *V* points plotted in Fig. 2 mark the actual maximum in the *V* band. Lacking *B*-band data for the maximum, the $E(B-V)$ reddening can be estimated only from $B-V$ colour at t_2^V, providing $A_V = 3.66$ from equation (1). From this and the extremely fast decline times listed in Table 3, the distance to this nova would be uncomfortably large, ≥30 kpc, placing it far beyond the Galactic bulge against which it is seen projected, at a hight of ≥2 kpc above the Galactic plane. This is clearly an unlikely location.

The $B-V$ colour measured for this nova at t_2^V seems to be strongly influenced by the presence of the cool giant, the severe crowding and the contribution by recombining flash-ionized wind of the companion, to the point of fooling the comparison with van den Bergh & Younger (1987) intrinsic colours. For similar reasons, the brightness at 15 d ($V = 16.35$ mag) appears to be useless for estimating the distance. If, for the extinction, we adopt instead the values given by SFD98 and SF11 and reported in Table 3, the distance to the nova is 5.4 and 9.4 kpc, respectively. In Table 3, we list the average 7.4 kpc value, which is compatible with a partnership to the Galactic bulge.

It is worth noting that the light curve of V1534 Sco displays a distinctive hiccup marked by the red arrow in Fig. 2. Its strength is wavelength-dependent, decreasing from the *B* to the *I* band. For sake of discussion, we have fitted the *V*-band light curve of V1534 Sco with the combination of two sources: the flash-ionized wind of the cool giant and the expanding nova ejecta. The latter is obtained as the difference (computed in flux space) between the observed light curve and the exponential decline from the flash-ionized wind.

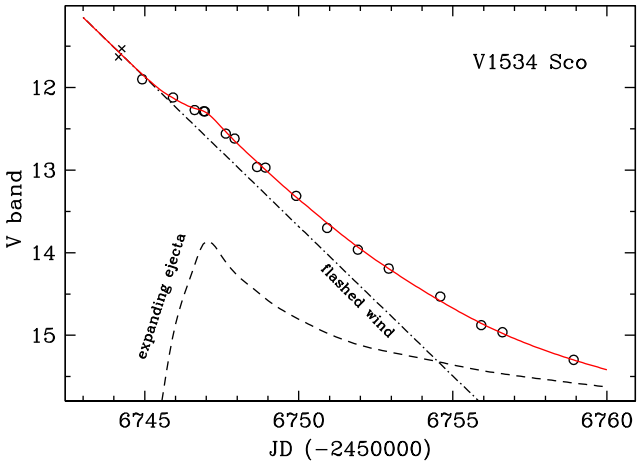

Figure 3. Fit to the *V*-band light curve of V1534 Sco (from Fig. 2), deconvolved into the light curve of the expanding ejecta and that of the recombining wind of the cool giant (for an e-folding time of 3 d) ionized by the initial flash of the nova (see Section 4.2.1 for details).

In Fig. 3, we present the results for a recombination e-folding time of 3 d, corresponding to an electron density of 1.5×10^7 cm^{-3} at the peak of the ionization and assuming an electron temperature of 10 000 K. The fit looks excellent, but this is hardly proof of its uniqueness. Given the fact that the near-IR observations by Joshi et al. (2015) did not detect a deceleration of the ejecta, it makes sense to treat the light curve derived in Fig. 3 for the expanding ejecta as that of the nova proper. In this case, the *V*-band maximum was reached on JD = 245 6747.0 at magnitude ∼13.8, with a decline rate $t_2^V \sim 13$ d. Adopting the larger extinction from SFD98, the distance (∼10 kpc) would still be compatible with a partnership to the bulge (the fainter apparent magnitude is compensated for by a similarly fainter absolute value implied by the slower decline rate).

4.3 V1535 Sco

V1535 Sco (= Nova Sco 2015 = PNV J17032620–3504140) was discovered by T. Kojina on 2015 Feb 11.837 (CBET 4078) and soon confirmed spectroscopically by Walter (2015) as an He/N nova. Nelson et al. (2015) performed X-ray and radio observations within a few days of discovery, and found the initial presence of hard, absorbed X-rays and synchrotron radio emission, which suggested that the nova erupted in a symbiotic binary, with a collision between the ejecta and the cool giant wind shock-heating plasma and accelerating particles. The suggestion of the presence of a cool giant companion was made also by Walter (2015). The synchrotron radio component rapidly declined during the following days while more conventional thermal free–free emission emerged (Linford et al. 2015), until synchrotron emission re-emerged at later times (Linford et al. 2017). Near-IR spectral monitoring by Srivastava et al. (2015a, 2015b) revealed a progressive narrowing of the never-too-broad emission lines from FWHM ∼ 2000 down to 500 km s^{-1}, indicating a decelerating shock as the nova ejecta collide with and are slowed down by the wind of the giant companion. Optical spectroscopy by Linford et al. (2017) shows a similar sharpening of the Hα profile during the early outburst phases. The extra brightness of the progenitor in quiescence Hα Super-COSMOS images was taken by Srivastava et al. (2015b) as further evidence of a symbiotic nature. Linear polarization measurements in the *BVRI* bands at seven consecutive dates in February were reported by Muneer, Anupama

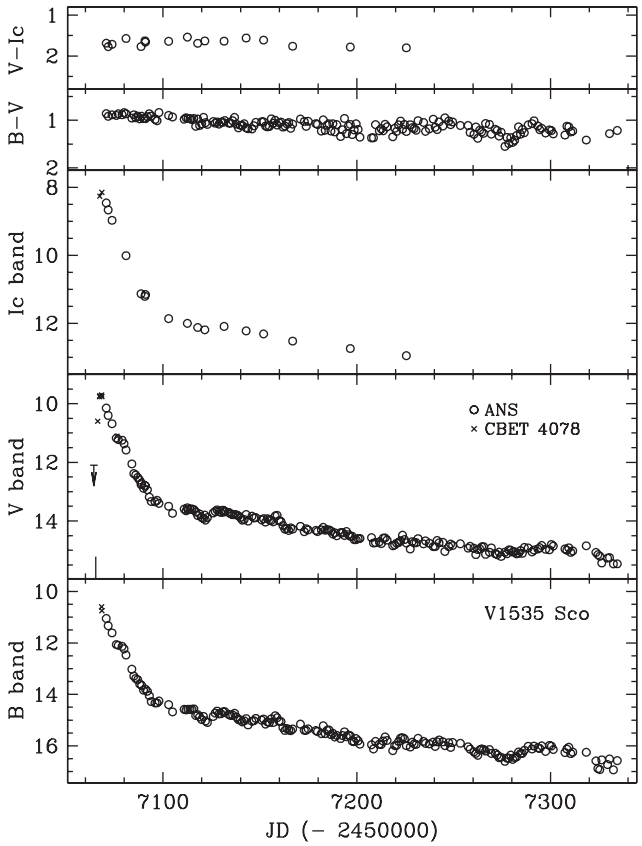

Figure 4. *BVI* photometric evolution of V1535 Sco (= Nova Sco 2015 = PNV J17032620–3504140). The solid vertical line in the *V*-band panel marks the time of nova discovery.

& Raveendran (2015) who concluded that, even if not corrected for interstellar polarization, the data support intrinsic polarization.

4.3.1 The light curve

The light curve resulting from our year-long monitoring of V1535 Sco is presented in Fig. 4, and the basic nova parameters are summarized in Table 3.

The overall light curve of V1535 Sco looks standard, with a faster decline during the initially optically thick conditions followed by a slower descent during the later optically thin phase. The transition from optically thick to thin ejecta occurred 27 d past and Δmag = 3.60 below the *V*-band maximum. Such a well-behaving transition is usually seen in Fe II novae (e.g. McLaughlin 1960), but much less frequently in He/N novae. The latter usually expel less material at larger velocity and higher ionization compared to Fe II counterparts, and their ejecta reach optically thin conditions much closer to maximum brightness.

A noteworthy feature of the light curve is the temporary dip that the nova went through around April 8 (JD = 245 7121), which developed at constant colours during the optically thin phase, as if for some time the ejecta were exposed to a lower flux of ionizing photons from the central source. A second, wider, and stronger dip, which occurred in mid-September (around JD = 245 7280), was instead strongly colour-dependent. Their interpretation would require access to detailed spectroscopic monitoring that we lack. Overall, the light curve of V1535 Sco during the optically thin phase has been 'bumpy', well beyond the measurement errors.

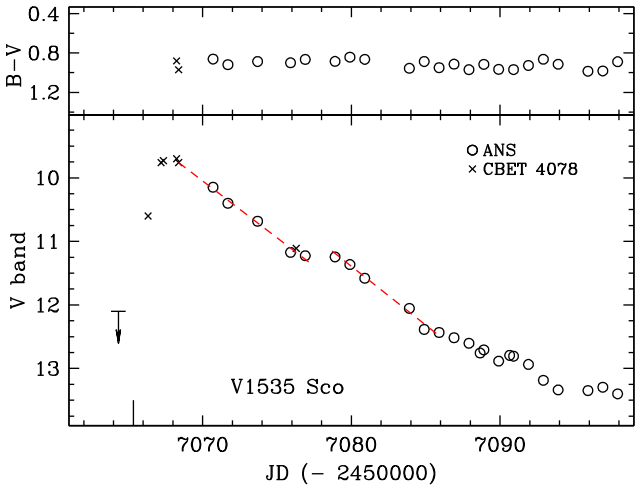

Figure 5. A zoomed portion around the maximum of the *V*-band light curve of V1535 Sco (= Nova Sco 2015 = PNV J17032620–3504140) from Fig. 4. The solid vertical line marks the time of nova discovery, and the upper limit is from CBET 4078 ported to the *V* band. The dashed lines aim to highlight the plateau around JD = 245 7078, which is discussed in Section 4.3.1.

Fig. 5 zooms in on the early portion of the *V*-band light curve, to highlight the plateau lasting a couple of days around Feb 24, or 10 d past and 1.5 mag below optical maximum. Two possible interpretations come to mind, but both have their share of problems.

First, the plateau could represent the same type of transition discussed in Fig. 3 for V1534 Sco, namely the emission from expanding ejecta overtaking that of the flash-ionized wind of the cool companion. This contrasts with the long delay past maximum, requiring a rising time to maximum for the ejecta ($\geq$10 d) which is more typical of Fe II events than He/N, for which it is generally an order of magnitude faster. This could be counter-argued by noting that (i) the initial He/N spectral classification for V1534 Sco could have been fooled by the dominating emission from the flash-ionized wind, and (ii) the narrowness of the emission lines, their Gaussian-like shapes and the presence of P-Cyg absorptions observed in the near-IR by Srivastava et al. (2015b) are more typical of Fe II novae, while He/H novae tend to show much broader and rectangular emission lines with no P-Cyg absorption components (Banerjee & Ashok 2012). It will be interesting to carefully inspect, when they are eventually published, optical spectra taken over a protracted interval of time to ponder the spectral classification of the expanding nova ejecta separately from that of the flash-ionized wind.

Secondly, a similar plateau has sometimes been observed in novae during the super-soft phase, when optically thin ejecta are exposed to the hard radiation field of the central WD still undergoing nuclear burning at its surface. The consequent input of ionizing photons spreading through the ejecta counter-balances the recombination of ions. The plateau is usually terminated either by rapid dilution in fast expanding and low-mass ejecta (as observed during the 2016 outburst of the recurrent nova LMC 1968; Munari et al. 2016a) or by switching off the nuclear burning on the WD (as in U Sco; Osborne et al. 2010). The problem in this case is that the plateau occurred two weeks before the ejecta turned optically thin on day 27 past optical maximum. One way out could be a highly structured, non-spherical shape of the ejecta, with optical thickness strongly dependent on angular coordinates. Hints in favour of such an arrangement are the fact that the nova erupted within the pre-existing wind of the giant companion, and optical (Walter 2015) as well as near-IR (Srivastava

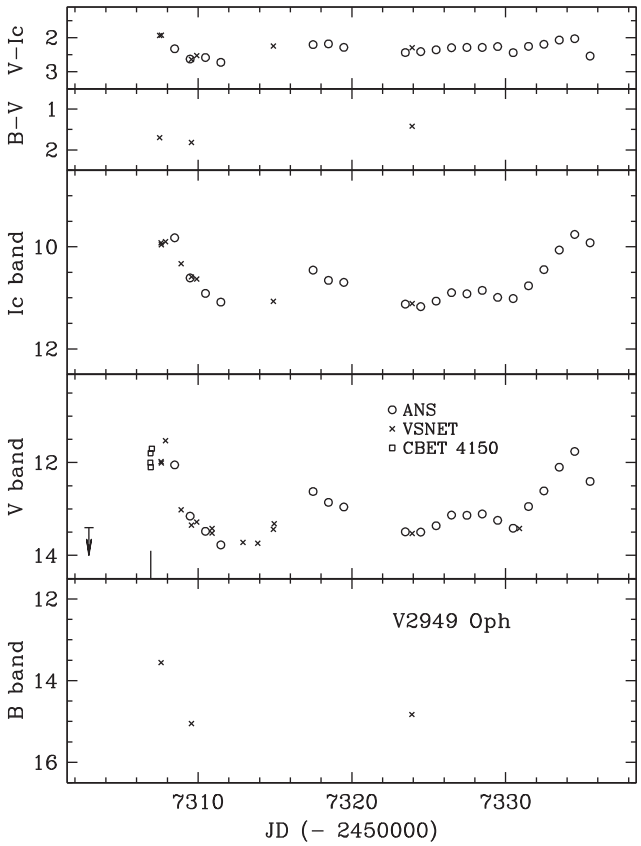

Figure 6. *BVI* photometric evolution of V2949 Oph (= Nova Oph 2015 N.2 = TCP J17344775–2409042). Data from CBET 4150 are reported as open squares and upper limit. The solid vertical line in the *V*-band panel marks the time of nova discovery.

et al. 2015b) spectra, which present weak emission components separated from the corresponding main ones.

The reddening estimated from nova colours and the total extinction along the line of sight deduced from the maps of SFD98 and SF11 are in excellent agreement (Table 3), and the derived distance places V1535 Sco at the distance of the Galactic bulge against which it is seen projected.

4.4 V2949 Oph

V2949 Oph (= TCP J17344775–2409042 = Nova Oph 2015 N.2) was discovered on 2015 Oct 11.41 by K. Nishiyama and F. Kabashima (CBET 4150), and confirmed spectroscopically on Oct 12.42 by Ayani (2015). Low expansion velocity, heavy reddening and a Fe II spectral class were reported by Campbell et al. (2015) from Oct 11 spectroscopic observations, while from Oct 11.99 observations Littlefield & Garnavich (2015) estimated as 900 km s^{-1} the FWHM of Hα emission and -800 km s^{-1} the velocity of its P-Cyg absorption component.

4.4.1 *The light curve*

Our light curve for V2949 Oph is presented in Fig. 6. We began the observations as night settled on Oct 12.98, soon after spectroscopic confirmation was circulated, and continued them until Nov 9, when solar conjunction prevented further data from being collected. This is the only programme nova that was not observed also in the *B* band.

The light curve shows the nova fluctuating by $\Delta V \sim 2$ mag around maximum brightness. Similar peak brightness was reached on Oct 12.38 at $V = 11.41$ and on Nov 7.99 at $V = 11.76$. The first has been taken – somewhat arbitrarily – as the true maximum, so that the brightness 15 d past it can be used to estimate a distance of 8.4 kpc (see Table 3), which places the nova right at the distance of the Galactic Centre. The reddening resulting from $B - V$ colour around maximum (see Fig. 6) indicates an extinction $A_V \sim 4.9$, uncomfortably in excess of the total value along the line of sight $A_V \sim 3.39$ from SFD98 maps and $A_V \sim 2.88$ from SF11 maps. Because the very few *B* magnitudes used in this exercise are not ours and come instead from VSNET observers (who did not provide details of their data reduction procedures and adopted comparison sequence), we make no further use of these *B*-band data.

4.5 V3661 Oph

V3661 Oph (= PNV J17355050–2934240 = Nova Oph 2016) was discovered in outburst by H. Yamaoka on Mar 11.81 (CBET 4265). A preliminary spectroscopic classification as a nova was derived by Munari et al. (2016b) from a very low signal-to-noise (S/N) spectrum, with later infrared and optical spectra by Srivastava et al. (2016) and Frank et al. (2016) fixing the spectral class to Fe II. All three spectral sources concur on a highly reddened continuum, FWHM $\sim 1000/1400$ km s^{-1} for Balmer emission lines and a velocity separation of $\sim$950 km s^{-1} between the emission and absorption components of the P-Cyg profile affecting most of the lines. A pre-discovery OGLE-IV observation at $I = 12.15$ on March 8.31 was reported by Mróz & Udalski (2016a) who noted the absence of the progenitor in OGLE deep template images, meaning it was fainter than 22 mag in the *I* band. A pre-discovery observation by ASAS-SN of the nova on March 10.85 has been noted by Chomiuk et al. (2016). Finally, Muneer & Anupama (2016) reported significant linear polarization in the *VRI* photometric observations of V3661 Oph obtained from March 13 to 19, which they interpret as arising primarily in the interstellar medium given the high reddening suffered by the nova.

4.5.1 *The light curve*

Our light curve for V3661 Oph is presented in Fig. 7, and the basic nova parameters are summarized in Table 3, as for the other programme objects.

The light curve looks particularly well behaving, almost a textbook example for a Fe II nova. The clear dependence on wavelength of the time of maximum brightness is discussed later in Section 5, in parallel with the similar case for TCP J18102829–2729590. The transition from optically thick to thin ejecta occurred 6.0 d past and Δmag = 3.35 below the *V*-band maximum.

With $t_2^V = 3.9$ and $t_3^V = 5.7$ d, V3661 Oph is probably the fastest known nova of the Fe II type, and a very fast one even compared with He/N recurrent novae such as U Sco. It is by far the nova with the reddest colours and therefore the highest extinction among the programme novae, with a mean observed colour $B - I \sim 6.25$, as averaged along the whole light curve. SFD98 and SF11 maps also suggest an extremely large total extinction along the line of sight to V3661 Oph. Finally, the short distance derived for this nova places it much closer than the bulge and within the Galactic disc.

4.6 MASTER OT J010603.18–744715.8

MASTER OT J010603.18–744715.8 was discovered (at unfiltered 10.9 mag) on 2016 Oct 14.19 by the MASTER-OAFA autodetection

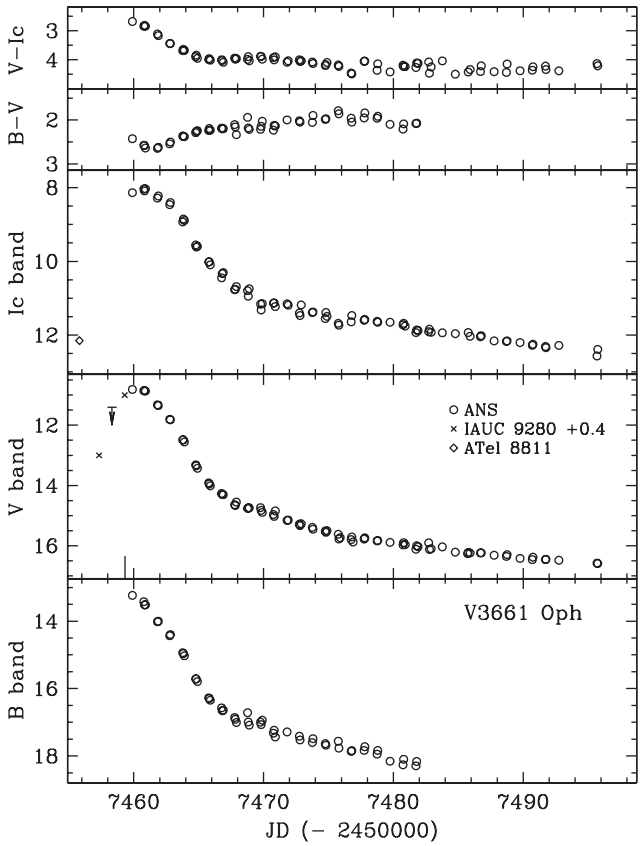

Figure 7. *BVI* photometric evolution of V3661 Oph (= Nova Oph 2016 = PNV J17355050–2934240). The data from IAUC 9280 (including the upper limit) refer to unfiltered observations, which have been shifted by 0.4 mag to fit the *V*-band light curve. The solid vertical line in the *V*-band panel marks the time of nova discovery.

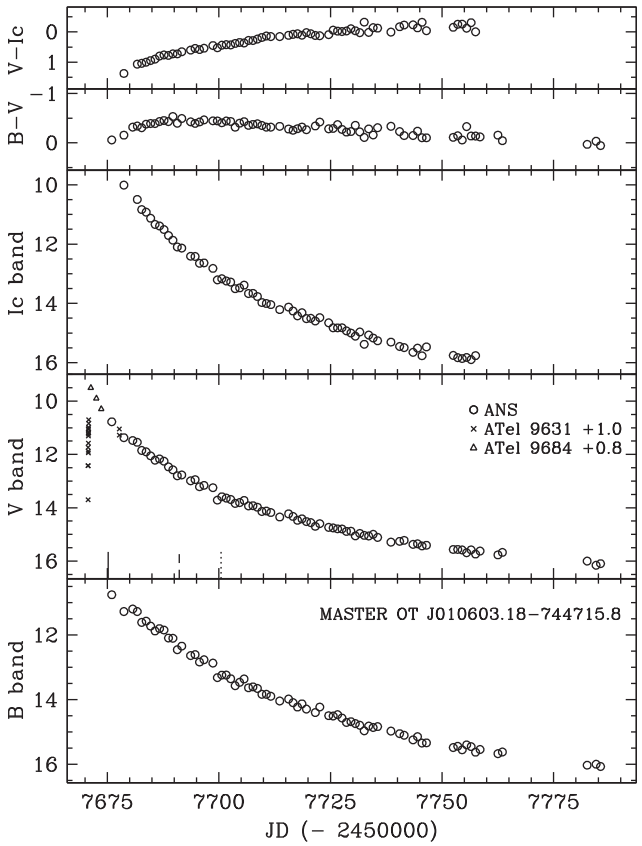

Figure 8. *BVI* evolution of MASTER OT J010603.18–744715.8 (= Nova SMC 2016). The solid, dashed and dotted vertical lines in the *V*-band panel mark respectively: the announcement of the nova by Shumkov et al. (2016), the appearance of nebular emission lines in optical spectra according to Williams & Darnley (2016b) and the emergence of super-soft X-ray emission following Page at al. (2016). Pre-discovery unfiltered data from Lipunov et al. (2016) and Jablonski & Oliveira (2016) are plotted on the *V*-band light curve after applying the offsets indicated (in mag; see Section 4.6.1 for details).

system and announced by Shumkov et al (2016) on Oct 14.34. ANS Collaboration monitoring began on Oct 14.51. Detection of the progenitor at mean $I = 20.84$ and $(V - I) = +0.16$ on archive OGLE-IV observations was reported by Mróz & Udalski (2016b), with hints of semiregular variability of a time-scale of 20–30 d.

Lipunov et al. (2016) found pre-discovery MASTER images that show how the nova was already declining from maximum when first noticed. An image for Oct 9.81 recorded the nova at (unfiltered) 8.5 mag, declining to 8.9 mag on Oct 11.07 and 9.3 mag on Oct 12.16. Robotic DSLR-camera monitoring of the SMC was inspected by Jablonski & Oliveira (2016) to obtain the (unfiltered) brightness profile of the rise towards maximum of the nova during Oct 9. The nova was fainter than 13.2 mag on Oct 9.197, first detected at 12.9 mag on Oct 9.210 and last measured at 9.90 mag on Oct 9.325.

Spectroscopic confirmation was obtained by Williams & Darnley (2016a) on Oct 14.70. They measured FWHM $\sim 3700\,\mathrm{km\,s^{-1}}$ for Balmer lines and classified the nova type as He/N. Following their description of the observed emission lines, the signatures in favour of the He/N class appears weaker than typical for this type, with some room left for a Fe II classification. Williams & Darnley (2016b) reported on their continued spectroscopic monitoring of the nova unil Oct 29, noting the disappearance of P-Cyg absorptions and the emergence of He I 5876, 7065 and of [O III] 4959/5007, from which they infer that the nova had entered the nebular phase. It should be noted that the presence of He I emission lines at the time [O III] emerges is standard for Fe II novae, and that the presence of P-Cyg absorption and [O III] nebular lines are more typical of Fe II than He/N novae (Williams 1992). In addition, the FWHM $\sim 3700\,\mathrm{km\,s^{-1}}$ observed for Balmer lines is close to the low limit for typical He/N novae while still well suited to Fe II novae.

The nova MASTER OT J010603.18–744715.8 has been intensively monitored in X-rays. Early *Swift* observations on Oct 15 failed to detect X-ray emission (Kuin et al. 2016). Rapidly brightening soft X-ray emission was detected by *Swift* starting with Nov 7 (Page et al. 2016). *Chandra* observations for Nov 17–18 (Orio et al. 2016a) confirmed the super-soft bright emission, which continued well into the *Chandra* observation for 2017 Jan 4 (Orio et al. 2016b), when a preliminary fit to the spectra supports an increase from 650 000 to 750 000 K for the temperature of the WD.

4.6.1 The light curve

The light curve of MASTER OT J010603.18–744715.8 is particularly simple and smooth, and it is presented in Fig. 8, with the basic parameters extracted from it summarized in Table 3. Fig. 9 zooms in on the phase of maximum, which was very brief with an extremely fast rise towards it, as pre-discovery observations by Lipunov et al. (2016) and Jablonski & Oliveira (2016) help to constrain. These unfiltered observations (i.e. white light, and therefore

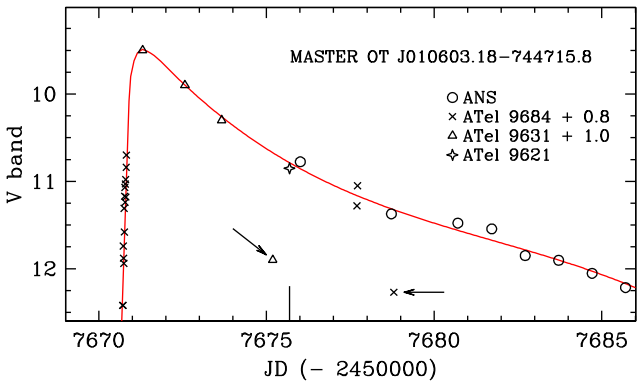

Figure 9. A zoomed portion around the maximum of the *V*-band light curve of MASTER OT J010603.18–744715.8 from Fig. 8. The solid vertical line marks the time of nova discovery. The continuous line is a polynomial fit to the data to guide the eye. The arrows point to discordant data from ATel 9631 and ATel 9684, as discussed in the text.

strongly skewed towards red wavelengths where CCD sensitivity peaks) require a large colour correction to be properly plotted on the *V*-band plane, because of the remarkably blue colours for the nova resulting from the very low reddening towards the SMC. The colour corrections are given in Fig. 9, and have been derived by continuity in comparison with our properly calibrated photometry. The latest observations listed by both Lipunov et al. (2016) and Jablonski & Oliveira (2016) are clearly off the otherwise well-behaving light curve of the nova (the two arrows in Fig. 9 point at these), and are ignored as erroneous data.

4.6.2 Super-soft X-rays and rate of decline

Our *BVI* data are transformed into absolute fluxes (erg cm^{-2} s^{-1}) and log–log plotted against time in the left panel of Fig. 10. For comparison, the same is done in the right panel for Nova Mon 2012 (data from Munari et al. 2013). The shaded area in the figure marks the time after the super-soft X-ray emission had ceased (Nelson et al. 2012; Page et al. 2013). The phase of super-soft X-ray emission corresponds to optically thin ejecta permeated by the hard radiation from the central WD undergoing stable nuclear burning at its surface (Krautter 2008; Schwarz et al. 2011). Such ionizing radiation partially counter-balances the recombination in the expanding ejecta, keeping high their emissivity and flattening the decline rates. When, with the end of the super-soft phase, this hard radiation input ends, the emissivity of the ejecta rapidly settles on to the pure recombination rate $\propto t^{-3}$, which is precisely what Nova Mon 2012 duly did. For MASTER OT J010603.18–744715.8, as soon as it entered the nebular phase and super-soft X-ray emission emerged (Page et al. 2016; Williams & Darnley 2016b), the decline in flux rapidly settled on a rate kept stable for all the period covered by our observations: $\propto t^{-1.8}$, $\propto t^{-1.6}$ and $\propto t^{-2.2}$, for *B*, *V* and *I*, respectively. The rates are slightly different from band to band, depending on the fractional contribution of continuum and emission lines, which decline at different speeds as the degree of ionization and electron density changes through the ejecta. The fact that these rates are much flatter than $\propto t^{-3}$ is interpreted as evidence that nuclear burning was still up and running on the surface of the central WD at the time of our last observations. When the nuclear burning does eventually end, it is expected that the decline in brightness of MASTER OT J010603.18–744715.8 will accelerate to $\propto t^{-3}$, as seen in Nova Mon 2012.

4.7 TCP J18102829–2729590

TCP J18102829–2729590 was discovered on 2016 Oct 20.383 at 10.7 mag by K. Itagaki (CBET 4332). Mróz, Udalski & Pietrukowicz (2016a) derived astrometric coordinates from OGLE-IV *I*-band images as RA = 18$^{\rm h}$10$^{\rm m}$28$^{\rm s}$.29 and Dec. = −27°29′59″.3, and noted that the progenitor is undetected in pre-outburst OGLE deep template images, meaning $I > 22$ mag. Spectroscopic classification as a Fe II class nova was obtained by Lukas (2016). The γ-ray emission from this nova has been detected by *Fermi*-LAT (Li & Chomiuk 2016).

4.7.1 The light curve

Our daily-mapped light curve of TCP J18102829–2729590 is shown in Fig. 11. It extends over a whole month and fully covers the phase of maximum brightness and decline well past t_3^V. It is smooth and characterized by a rapid initial rise and two distinct maxima. Our monitoring was stopped by solar conjunction when the nova was still bright. As for the other novae, the parameters extracted from the light curve are listed in Table 3. The distances derived from t_2^V, t_3^V and V_{15} are dependent on which of the two maxima is taken as reference. The average of the values listed in Table 3 is 8.1 kpc, like that of the bulge against which the nova is seen projected. The partnership to the bulge is confirmed by the photometric reddening of the nova, which equals the total extinction along the line of sight from the 3D maps of SFD98 and SF11.

There is a striking difference between the two maxima displayed by TCP J18102829–2729590: the first is markedly wavelength-dependent, and the other is not.

The wavelength dependence of the first maximum manifests in a time delay of ∼1 d between peak brightness in the *B* and *I* bands, as noted above for V3661 Oph. As discussed in Section 5, this is a characteristic of the initial fireball expansion of the ejecta, with the maximum representing the time of largest angular extension for the pseudo-photosphere that is optically thick at the given wavelength. The independence from wavelength of the second maximum suggests it is of a different physical nature, which is discussed later in Section 6.

4.8 ASASSN-16ma

ASASSN-16ma was discovered at $V \sim 13.7$ in ASASSN-CTIO images obtained on 2016 Oct 25.02, brightened to $V \sim 11.6$ a day later, and it was undetected ($V > 17.3$) on Oct 20.04 (Stanek et al. 2016). Its coordinates were originally given as RA = 18$^{\rm h}$20$^{\rm m}$52$^{\rm s}$.12 and Dec. = −28°22′13″.52, which Saito et al. (2016) adopted to identify the likely progenitor in the VVV Survey, as a source possibly consisting of two unresolved components of combined brightness $z = 18.8$, $Y = 18.5$, $J = 18.1$, $H = 17.8$ and $K_{\rm s} = 17.6$ mag. Mróz et al. (2016a) remeasured the position of the nova on OGLE-IV *I*-band images and derived a different astrometric position, RA = 18$^{\rm h}$20$^{\rm m}$52$^{\rm s}$.25 and Dec. = −28°22′12″.1, which is 2.4 arcsec away from the initial ASASSN-CTIO position. The progenitor is not visible in pre-outburst OGLE-IV survey images, meaning that this was fainter than $I > 22$ mag; therefore, the star proposed by Saito et al. is an unrelated field star.

A low-resolution spectrum obtained on Oct 27.5 by Luckas (2016) showed the object to be a Fe II class nova. A month later, on Nov 23.1, Rudy, Crawford & Russell (2016) obtained an optical/near-IR spectrum of ASASSN-16ma that confirmed the Fe II classification and was characterized by prevailing low-expansion

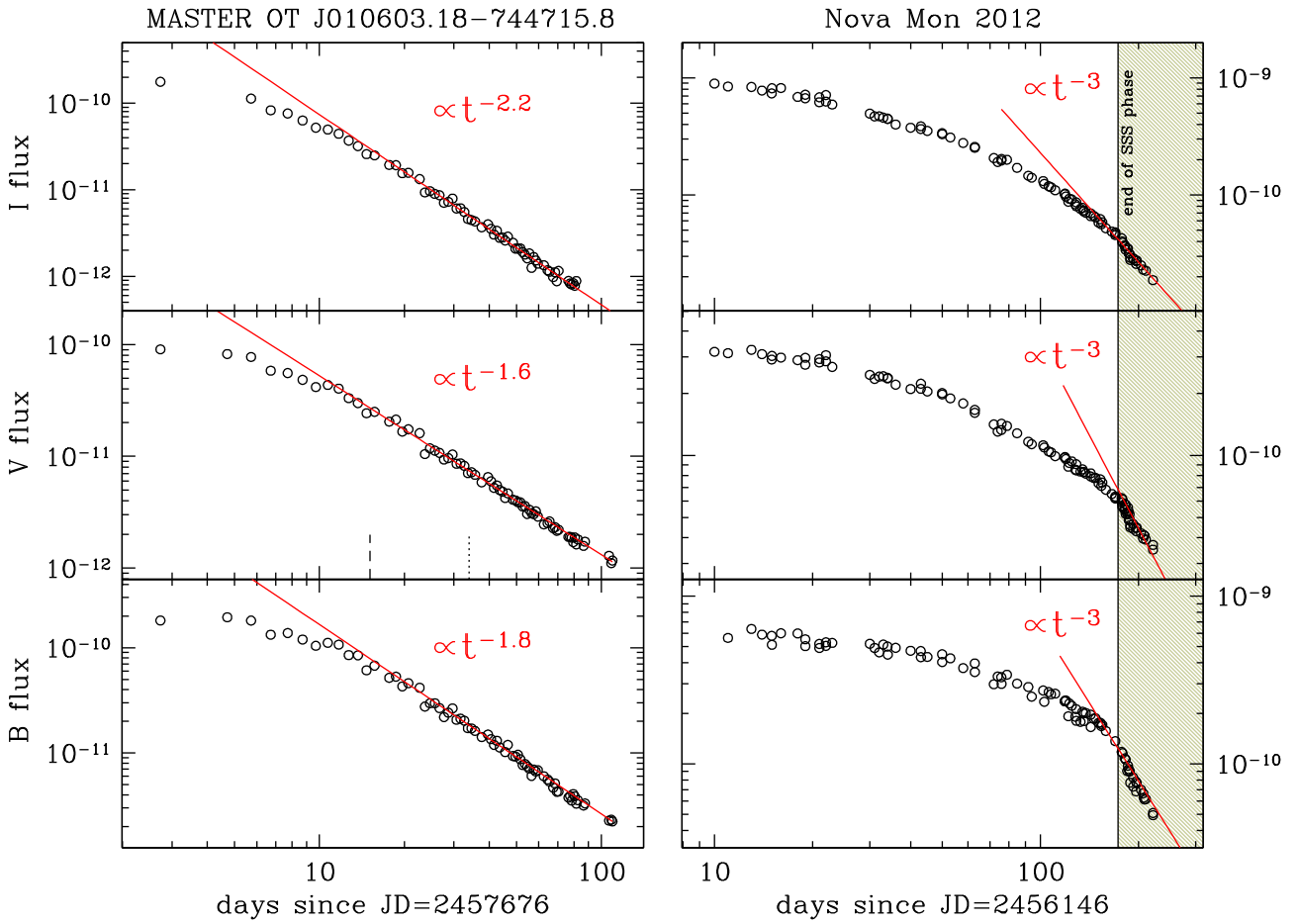

Figure 10. Left: evolution of flux through *BVI* bands for MASTER OT J010603.18–744715.8 (= Nova SMC 2016). The lines are linear fits to flux at later epochs, providing the indicated decline rates. The dashed and dotted vertical lines in the *V*-band panel mark, respectively, the appearance of nebular emission lines in optical spectra (Williams & Darnley 2016b) and the emergence of super-soft X-ray emission (Page at al. 2016). Right: the same for Nova Mon 2012 (data from Munari et al. 2013) to highlight the change in the slope following the end of the super-soft phase and thus the end of nuclear burning on the central WD (shadowed region to the right).

velocity and low-excitation conditions. The γ-ray emission from ASASSN-16ma was discovered by Li, Chomiuk & Strader (2016a) while they were monitoring with *Fermi*-LAT the nearby nova TCP J18102829–2729590, described in Section 4.7. ASASSN-16ma remained undetected by *Fermi*-LAT until Nov 8 (JD = 245 7701) when it suddenly turned into a strong γ-ray source, remaining active (although declining) for the following 9 d (Li et al. 2016b).

4.8.1 The light curve

Our daily-mapped light curve of ASASSN-16ma is shown in Fig. 12. It extends over a whole month and covers the initial rise, the phase of maximum and decline well past t_3^V. Our monitoring was stopped by solar conjunction when the nova was still bright. A zoomed view of the initial rise in brightness is given in Fig. 13, where our *V*-band observations are combined with data from the literature.

The light curve of ASASSN-16ma started as a simple one. The two observations for Nov 4.0 and 5.0 (JD = 245 7696.5 and 245 7697.5) are highlighted by filled dots in Fig. 12. They are characterized by the same dependence on wavelength as for the maximum brightness of V3661 Oph (Fig. 7) and the first maximum of TCP J18102829–2729590 (Fig. 11), namely a time delay of ∼1 d between the maximum in the *B* and *I* bands. We believe these filled dots trace the normal fireball maximum that ASASSN-16ma initially went through. In support of this interpretation, it is worth noticing that for the two γ-ray programme novae, both belonging to the bulge and affected by a similarly low reddening, the first maximum occurred at a similar brightness: $V = 8.1$ for ASASSN-16ma and $V = 7.6$ for TCP J18102829–2729590. The hiccup around Nov 1.0 (JD = 245 7693.5) could mark the pre-maximum halt seen in some novae at a similar ∼1 mag below maximum (Hounsell et al. 2010).

Soon after the passage through the fireball maximum, ASASSN-16ma increased to a second and brighter maximum, composed of two peaks. As for TCP J18102829–2729590, the distance to ASASSN-16ma derived from t_2^V, t_3^V and V_{15} depends on which of these two peaks is taken as reference. Choosing the first one (at JD = 245 7700.5) returns a distance shorter than that of the bulge, with a larger distance when selecting the second (at JD = 245 7707.5). The average is 8.3 kpc, which also places ASASSN-16ma at the distance of the bulge against which the nova is seen projected. Similarly to TCP J18102829–2729590, the partnership to the bulge is confirmed by the photometric reddening of ASASSN-16ma, which

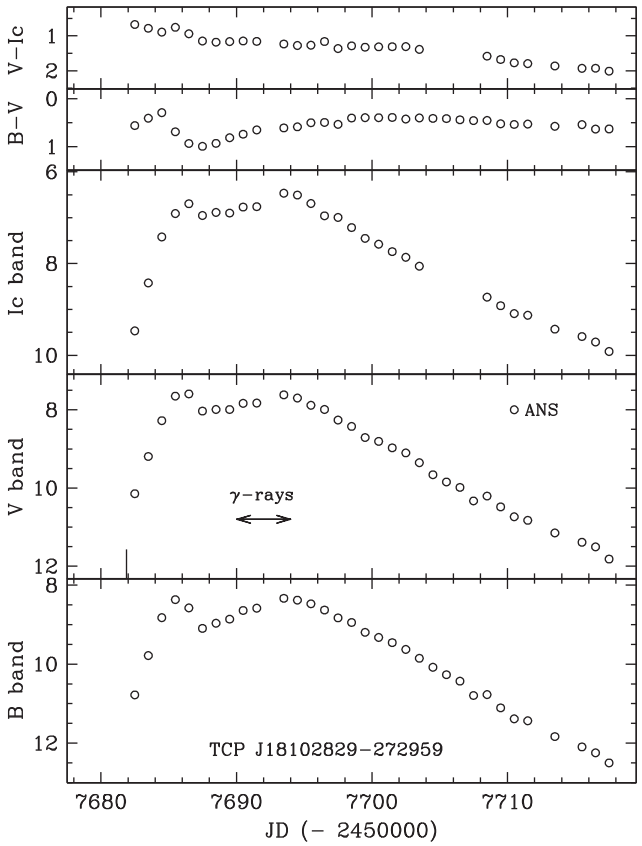

Figure 11. *BVI* photometric evolution of the nova TCP J18102829–2729590. The solid vertical line in the *V*-band panel marks the time of nova discovery. The left–right arrow highlights the time interval during which γ-ray emission from the nova was detected by *Fermi*-LAT (Li & Chomiuk 2016).

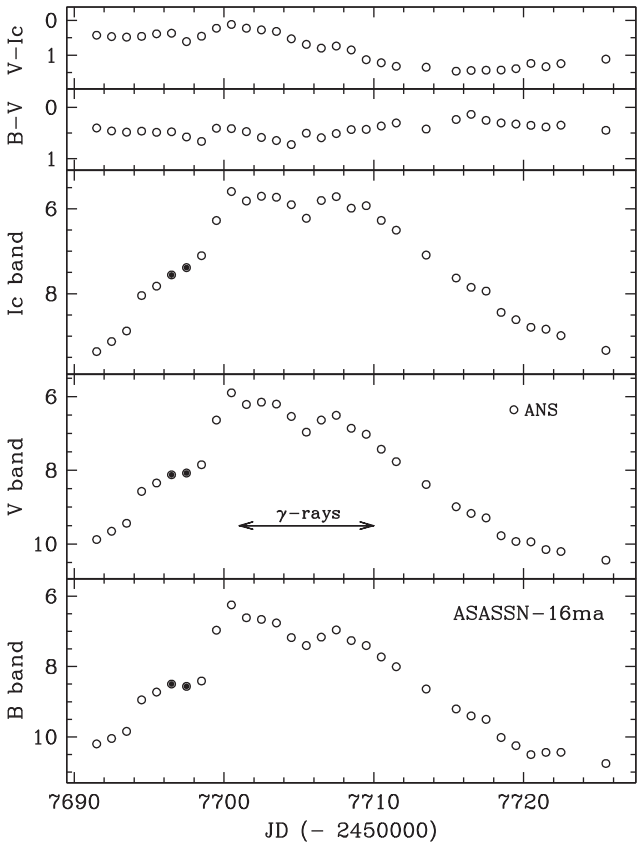

Figure 12. *BVI* photometric evolution of ASASSN-16ma. The left–right arrow marks the time interval during which γ-ray emission from the nova was detected by *Fermi*-LAT (Li et al. 2016a, b). For the meaning of the two filled dots (as also plotted in Fig. 15), see the text (Section 6).

equals the total extinction along the line of sight from the 3D maps of SFD98 and SF11. As for TCP J18102829–2729590, the second maximum displayed by ASASSN-16ma is discussed in Section 6.

5 THE FIREBALL EXPANSION

The initial photometric evolution of a nova is characterized by the rise towards maximum, the maximum itself and the settling on to decline. The rise towards maximum is rarely mapped at optical wavelengths (Seitter 1990), because it is usually very fast (a matter of a few days or even hours) and the discovery of the nova has a higher chance of occurring when the object is at peak brightness (especially so in crowded fields).

Nonetheless, sometimes the conditions are just right to cover the transit of a nova through optical maximum. For the seven programme novae, this is the case for TCP J18102829–2729590 and V3661 Oph, and marginally so for the others. Fig. 14 presents a zoom of their light curves around optical maximum. The obvious feature is how the maximum brightness occurs at later times with increasing wavelength.

The flux density emitted by the ejecta of the nova expanding as an homogeneous, ionized plasma is

$$f_\nu = B_\nu(d/D)^2(1 - \mathrm{e}^{-\tau_\nu}), \qquad (2)$$

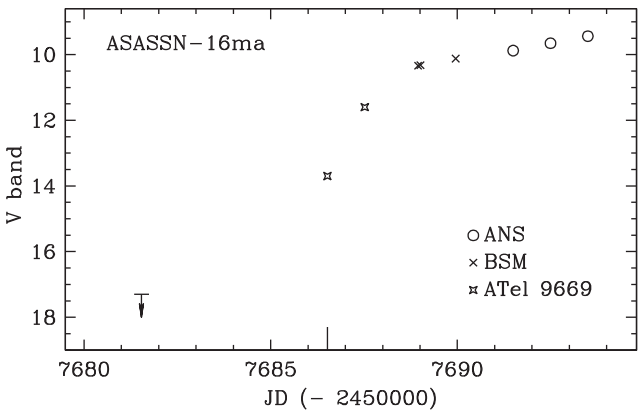

Figure 13. Zooming in on the early evolution of ASASSN-16ma. The solid vertical line marks the time of nova discovery. BSM is the AAVSO bright star monitor (by A. Henden).

where B_ν is the Planck function, d is the linear dimension of the ejecta that scales as $\sim v_{\rm ej}(t - t_\circ)$, D is the distance to the nova and τ_ν is the free–free optical depth from bremsstrahlung of electrons. Following Altenhoff et al. (1960) and Mezger & Henderson (1967), τ_ν is

$$\tau_\nu \approx 0.08235 T_{\rm e}^{-1.35} \nu^{-2.1} \int N_{\rm e}^2 \, {\rm d}l, \qquad (3)$$

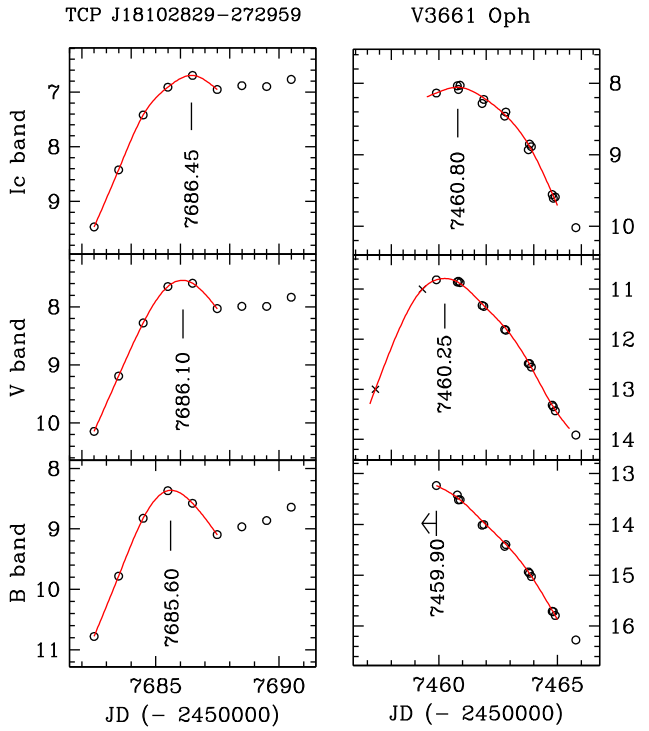

Figure 14. Wavelength dependence of the time of maximum brightness in novae TCP J18102829–2729590 and V3661 Oph.

where N_e and T_e are the electron density (cm^{-3}) and temperature (K), respectively, ν is the frequency in units of 10^9 Hz, and the emission measure $\int N_e^2\, dl$ is in pc cm^{-6}. The time delay between maximum brightness reached in different photometric bands can be expressed as

$$\begin{aligned}
t^V_{max} - t^B_{max} &= 0.35 \times \Theta \text{ (d)} \\
t^R_{max} - t^V_{max} &= 0.25 \times \Theta \\
t^I_{max} - t^V_{max} &= 0.70 \times \Theta \\
t^J_{max} - t^V_{max} &= 1.55 \times \Theta \\
t^H_{max} - t^V_{max} &= 2.15 \times \Theta \\
t^K_{max} - t^V_{max} &= 2.90 \times \Theta, \qquad (4)
\end{aligned}$$

with

$$\Theta = \left(\frac{T_e}{10^4\ \mathrm{K}}\right)^{-0.27} \left(\frac{M_{ej}}{10^{-4}\ \mathrm{M_\odot}}\right)^{+0.4} \left(\frac{v_{ej}}{1000\ \mathrm{km\ s^{-1}}}\right)^{-1}, \qquad (5)$$

where M_{ej} is the ejected mass and v_{ej} is the ejection velocity. This time delay is the same reason that the maximum thermal radio emission is reached ∼yr past optical maximum (Hjellming 1974). The timings given in Fig. 14 correspond to $t^I_{max} - t^B_{max} = 0.85$ and ≥0.90 for TCP J18102829–2729590 and V3661 Oph, respectively. This is close to what is expected from equation (4) for typical values of T_e, M_{ej} and v_{ej} adopted in computing Θ.

6 A SECOND LIGHT-CURVE COMPONENT PARALLELING THE EMISSION IN γ-RAYS

The light curve of the two γ-ray programme novae, TCP J18102829–2729590 and ASASSN-16ma, is characterized by the distinct presence of two components, which are highlighted in Fig. 15. The initial or fireball component produces a passage through the maximum that is dependent on wavelength, as described in the previous section. The second component appears at a later time and peaks simultaneously with the detection of the nova in γ-rays (for which reason, we call it the *gamma* component) and it gives origin to a second maximum that is not wavelength-dependent.

The gamma component of the optical light curve behaves synchronously with the emission observed in γ-rays. The preliminary analysis by Li et al. (2016b) of the daily averaged γ-ray behaviour of ASASSN-16ma shows a sudden detection coincident with peak flux on Nov 8 (JD = 245 7700.5) followed by a general decline along the following 9 d, with a significant 1-d γ-ray flux dip observed on Nov 13 (JD = 245 7705.5). The gamma component of the optical light curve in Fig. 15 presents exactly the same behaviour: a maximum on Nov 8 and a general decline for the following 9 d with a 1-d brightness dip centred on Nov 13. Not only the shapes but also the flux ratios behaved in parallel. In fact, during the 9 d of general decline, the γ-ray flux changed by a factor of 3, from 9.7 (±1.3) to 3.4 (±2.1) × 10^{-7} ph cm^{-2} s^{-1} (Li et al. 2016b); over the same period of time, the flux through the *V* band also declined by a factor of 3, from $V = 5.89$ to $V = 7.02$. Once the daily γ-ray behaviour of TCP J18102829–2729590 has become available, it will be interesting to explore if a similar degree of parallelism with the gamma component of its optical light curve was also followed.

As further evidence of the link between the γ-ray emission and the gamma component of the light curve, it is worth noticing that the reported mean γ-ray flux of ASASSN-16ma (Li and Chomiuk 2016) is 2.5× higher than for TCP J18102829–2729590 (Li et al. 2016b). The reddening-corrected mean flux of the gamma component of the two novae in Fig. 15 is exactly in the same 2.5× ratio, or $\langle(V)_\circ\rangle$ = 5.19 and $\langle(V)_\circ\rangle$ = 6.15 for ASASSN-16ma and TCP J18102829–2729590, respectively.

A difference of 2.5× in the mean γ-ray flux for the two programme novae, both belonging to the bulge, seems to disprove the common beliefs (e.g. Ackermann et al. 2014), that (i) the intrinsic γ-ray brightness is similar among normal novae, (ii) they can be detected by *Fermi*-LAT over only limited distances from the Sun, and therefore (iii) γ-ray emission is a widespread (if not general) property of novae. Judging from ASASSN-16ma and TCP J18102829–2729590, it appears instead that novae can be firmly detected by *Fermi*-LAT up to and beyond the Galactic bulge, and their intrinsic brightness in γ-rays can differ greatly. Combining this with the relatively low number of normal novae detected to date by *Fermi*-LAT (six novae in total have been detected in γ-rays, in contrast to the 69 discovered optically in the same period; see Morris et al. 2017), it is tempting to conclude that γ-ray emission is not a widespread property for them.

The two-component light curve described here for the programme γ-ray novae brings to mind the two-component ejecta adopted to model the radio-interferometric observations of some recent novae (Chomiuk et al. 2014; Weston et al. 2016); a faster polar wind collides with a slower (and pre-existing?) equatorial density enhancement. However, this scenario applies to radio observations extending for months past the initial eruption. The second or gamma component of the optical light curve of programme γ-ray novae develops instead within a few days of the initial fireball component, and could therefore trace something different in the kinematical and geometric arrangement of the ejecta. We postpone to a future paper a quantitative modelling of our two-component light curve for γ-ray novae, waiting for observations of these at other wavelengths to be published and including similar data for additional objects to reinforce the statistics.

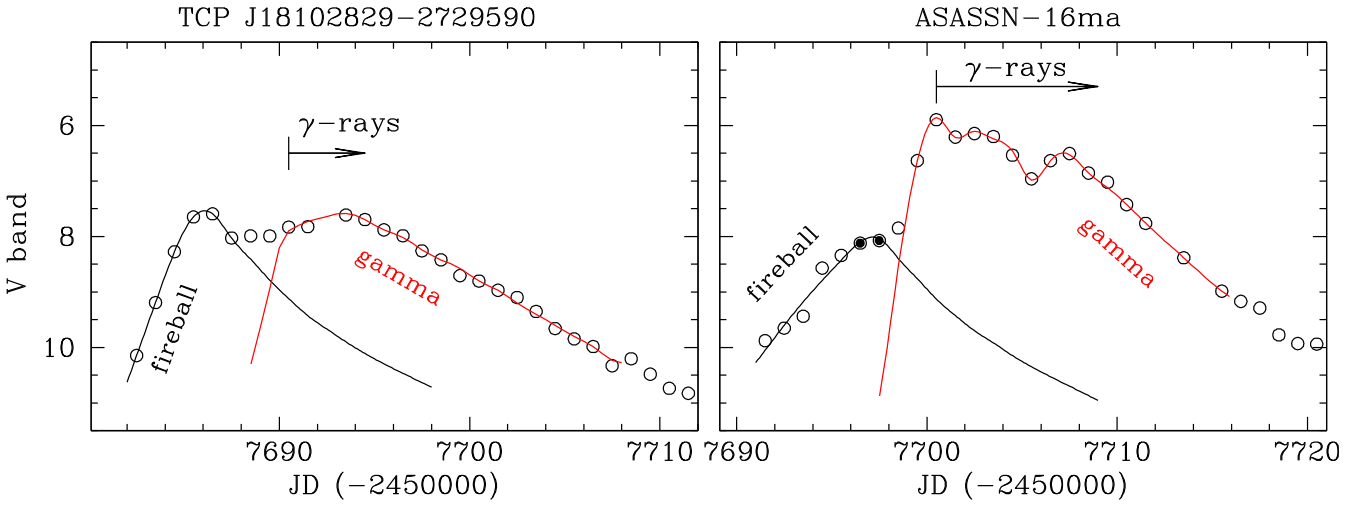

Figure 15. Deconvolution of the light curve of the two programme bulge novae detected by *Fermi*-LAT. The fireball component is the one associated with free ballistic expansion of ejecta (see Section 5). The gamma component appears and evolves in parallel with the emission detected in γ-rays (see Section 6). The filled dots are the same as in Fig. 12 The dip around JD = 245 7705 in the gamma component for ASASSN-16ma corresponds to a similar dip in the γ-ray flux recorded by *Fermi*-LAT (see Li et al. 2016b).

7 PROGENITORS

At the position of four programme novae, V2949 Oph, V3661 Oph, TCP J18102829–2729590 and ASASSN-16ma, no progenitor is visible in deep OGLE *I*-band images or DSS plates, which set the minimal outburst amplitudes listed in Table 3. For all of these, a progenitor containing a giant or a subgiant companion would have been brighter in the *K* band than the completeness limit of the 2MASS in the respective areas, suggesting that their donor star is a dwarf. For the remaining three programme novae (V1534 Sco, V1535 Sco and MASTER OT J010603.18–744715.8), a progenitor has been proposed based on positional coincidence with pre-outburst surveys. We consider in turn these three novae.

7.1 V1534 Sco

Joshi et al. (2014) proposed 2MASS 17154687–3128303 as the progenitor of the nova V1534 Sco. At $J = 11.255(\pm0.042)$, $H = 10.049(\pm0.039)$ and $K = 9.578(\pm0.035)$, it lies at 0.6 arcsec from the position of the nova reported by SIMBAD. By fitting with a blackbody only its 2MASS and *Wide-field Infrared Survey Explorer* (*WISE*) infrared energy distribution, Joshi et al. (2014) classified the star as an M5 III giant, reddened by $E(B-V) = 0.9$.

In Fig. 16, we present the observed SED of the progenitor of V1534 Sco. To the 2MASS *JHK* and *WISE* $W_1W_2W_3$ infrared data considered by Joshi et al. (2014), we add $I = 14.22$ mag from DENIS and $R = 17.20$ mag from the SuperCOSMOS catalogue. We have not been able to find quiescence *B* and *V* data. As noted in Section 4.2.1, at the latest stages the light curve of V1534 Sco became completely flat, with asymptotic values $B \sim 19.6$, $V \sim 18.3$ and $I \sim 14.3$. The latter is practically identical to the pre-outburst DENIS $I = 14.22$ mag value, suggesting that these asymptotic values could be viable proxies for the brightness in quiescence. Therefore, we added the asymptotic *B* and *V* values to the SED of Fig. 16, where we overplot to the nova the SEDs of G3 III–M6 III giants, compiling their optical/infrared intrinsic colours from Koornneef (1983), Bessell (1990) and Fluks et al. (1994). The SEDs of giants are reddened according to the total extinction along the line of sight to V1534 Sco (see Table 3) as derived from the 3D maps of SFD98 and SF11. We have already seen in Section 4.2.1 how these values for the extinction lead to a correct distance to the nova. They have been transformed into the corresponding $E(B-V)$ and A_λ following the relations calibrated by Fiorucci & Munari (2003) for M-type giants.

The best fit to *RIJHKW*$_1$*W*$_2$*W*$_3$ data in Fig. 16 is obtained via χ^2 with an M3 III for $E(B-V) = 1.63$ and an M1 III for $E(B-V) = 1.95$. Overall, the fit with M3 III is better. This is minimally dependent on $KW_1W_2W_3$ bands, while *RIJ* are far more relevant. The fit with M3 III provides a distance of 8.2 kpc, while that with M1 III drops to 5.0. Considering the partnership of the nova with the bulge, we conclude that the progenitor of the nova V1534 Sco is well represented by an M3 III cool giant reddened by $E(B-V) = 1.63$.

The *B* and *V* points lie above both fit attempts in Fig. 16. There are at least three suitable explanations for this: (i) the asymptotic *B* and *V* values are still influenced by emission from the nova ejecta; (ii) the severe crowding that fooled the derivation in Section 4.2 of $E(B-V)$ from nova photometry is also affecting the *B* and *V* brightness of the progenitor; (iii) ionization of the cool giant wind by the WD produces extra flux at *B* and *V* wavelengths. It is, in fact, well known that the *UBV* colours of symbiotic stars are much bluer than those of the M giants they harbour – see the *UBVRI–JHKL* photometric surveys of known symbiotic stars by Munari et al. (1992) and Henden & Munari (2008) – because of the contribution at shorter wavelengths by the emission from circumstellar ionized gas.

7.2 V1535 Sco

Srivastava et al. (2015b) proposed 2MASS 17032617–3504178 ($J = 13.40$, $H = 12.53$ and $K = 12.22$) as the progenitor. This star is positionally coincident to better than 0.1 arcsec with the nova, with a *Gaia* Data Release 1 source of $G = 14.392$ mag, and a DENIS counterpart with $I = 15.24$ mag.

In Fig. 17, we plot the observed SED for the progenitor of V1535 Sco, combining 2MASS *JHK* and *WISE W1W2* infrared data, to which we have added $I = 15.24$ mag from DENIS, $V = 17.05$ mag from the YB6 Catalog (USNO, unpublished; accessed via Vizier at

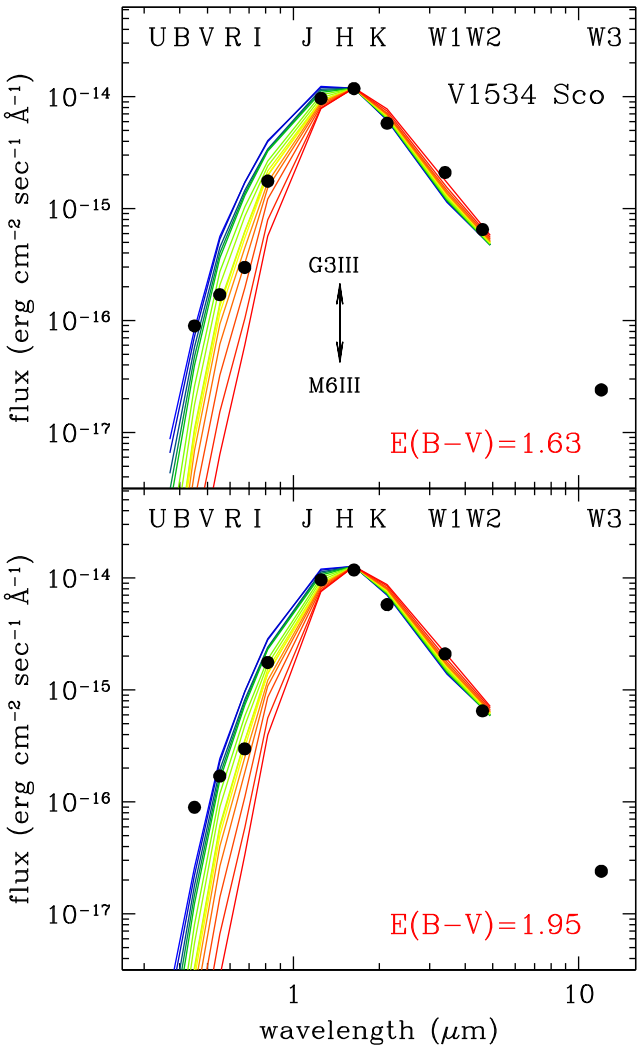

Figure 16. SEDs (black dots) of the progenitor of the nova V1534 Sco. The families of curves plot the energy distribution of giant stars reddened by $E(B-V) = 1.63$ and 1.95, corresponding to the extinction from the 3D maps of SFD98 and SF11, respectively. The giants go from G3 III to M6 III, and are scaled to fit the progenitor at the H band. Their SEDs are constructed by combining data from Koornneef (1983), Bessell (1990) and Fluks et al. (1994). The best fit (B and V bands excluded; see Section 7.1) is for an M3 III in the upper panel and M1 III in the lower panel.

CDS) and $R = 16.33$ from SuperCOSMOS. We have considered the fit with the same family of energy distributions of G3 III–M6 III giants already used in Fig. 16 for V1534 Sco, this time reddened by the same $E(B-V) = 1.03$ derived and discussed above for the nova. The fit is clearly unsatisfactory at optical wavelengths, implying blue intrinsic colours for the progenitor. At the distance given in Table 3 for the nova, the absolute magnitude of the progenitor would be $M(K) = -2.9$, which is that expected for a K3–4 III giant. Such a classification was one of the alternatives (the other being M4–5 III) considered by Srivastava et al. (2015b).

Although rare, the symbiotic stars with K giants account for ∼10 per cent of the total in the catalogue by Belczyński et al. (2000). The optical colours of some of them (see Munari et al. 1992; Henden & Munari 2008) are strongly affected by the blue emission of the K giant wind ionized by the radiation from the WD companion, and this could easily be a viable interpretation for the progenitor of V1535 Sco.

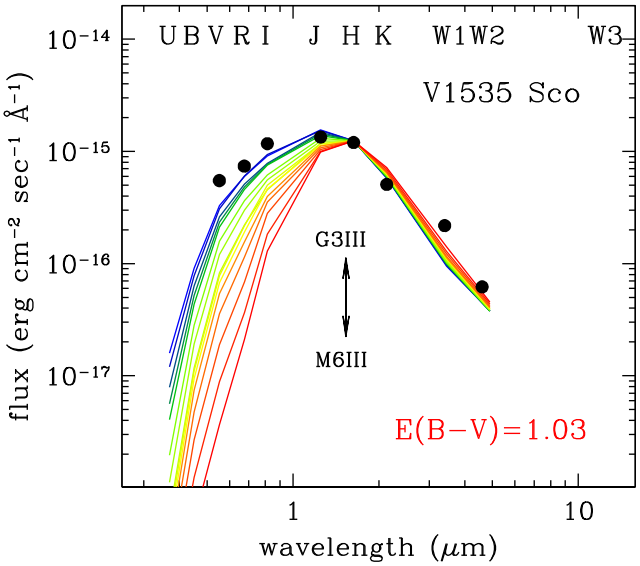

Figure 17. SEDs (black dots) of the progenitor of the nova V1535 Sco. The families of curves plot the energy distribution of giant stars reddened by $E(B-V) = 1.03$. All details as for Fig. 16.

7.3 MASTER OT J010603.18–744715.8

Mróz et al. (2016b) reported that the progenitor was clearly visible in OGLE-IV survey images at equatorial coordinates RA = $01^{h}06^{m}03^{s}.27$, Dec. = $-74°47'15''.8$ (J2000.0), $I = 20.84$ mean magnitude and $V - I = +0.16$ colour. They add that it showed semiregular variability on a time-scale of 20–30 d. The blue colour reflects into the non-detections by 2MASS and *WISE* infrared surveys.

At a distance of 1.03 arcsec from the OGLE position, there is a *Galaxy Evolution Explorer* (*GALEX*) source of magnitudes FUV = 20.529(±0.331) and NUV = 20.573(±0.205), the second closest *GALEX* source being 30 arcsec away. The astrometric proximity and compatible magnitudes and colours suggest that the OGLE and *GALEX* sources are the same star, of blue colours consistent with those of a disc-dominated source.

Adopting the $E(B-V) = 0.08$ reddening and 61 kpc distance to the SMC listed by Mateo (1998), the absolute magnitude of the progenitor is $M(V) = +1.8$, which suggests a subgiant as the donor star. A giant of the T CrB type would shine at $M_V \sim -0.5$ (Sowell et al. 2007), while the mean magnitude for novae with dwarf companions is $M_V \sim 4.5$ (Warner 1995). The presence of a subgiant is consistent with the non-detection of the progenitor during the 2MASS.

8 CONCLUSIONS

Optical multiband light curves can still play a vital role in the study of nova eruptions. To properly pursue this, they must be densely mapped with observations of the highest external photometric accuracy, which need to begin immediately with the announcement of the nova. To overcome the inevitable problems induced by the nova emission-line spectrum being convolved with the actual passband profiles realized locally, the entire light curve should be based on homogeneous data obtained with a single instrument and should not be the result of a combination of sparse data from a variety of different telescopes. Under such circumstances, any glitch in the

light curve will correspond to some real change in the physical conditions experienced by the nova.

The light curves of the programme novae have allowed us to detect and trace many subtle effects, such as the recombination of the flashed wind from a cool giant companion, the dependence on wavelength of the passage through the fireball maximum, the persistent reionization of ejecta during the X-ray super-soft phase, the time of its switch-off, as well as plateaus and hiccups of characteristic dependence on wavelength.

The careful application of MMRD relations to the high-quality light curves of this paper has returned consistent distances, with five novae (including the two detected in γ-rays) belonging to the Galactic bulge, one to the SMC and one to the Galactic disc. Also, the reddenings derived from proper $(B-V)$ colours at maximum and at t_2^V relate well to Galactic extinction maps such as those of SFD98 and SF11. Such reddenings have been key ingredients in fitting the pre-outburst energy distribution for the programme novae detected prior to their eruptions, which are objects with evolved companions.

Finally, the light curves of the two novae detected by *Fermi*-LAT have show the emergence of a second optical component in phase with the emergence of γ-rays. The time-behaviour of this second optical component strictly follows the evolution seen in γ-rays, including small up-and-downs superimposed on the general trend. The reddening-corrected flux radiated by the two novae in this additional component of their optical light curves scales as the ratio of their brightness in γ-rays. The presence of this second component in the light curve of γ-ray novae would possibly have been overlooked in a typical study dealing with only one object at a time. Instead, it stands out prominently in a comparative study like this present study based on data of the highest homogeneity for several novae, an approach we intend to pursue again in the future.

ACKNOWLEDGEMENTS

We would like to thank S. Dallaporta, F. Castellani, G. Alsini and R. Belligoli for some check observations carried out on the programme targets.

REFERENCES

Ackermann M. et al., 2014, Sci, 345, 554
Altenhoff W., Mezger P. G., Strassl H., Wendker H., Westerhout G., 1960, Veroff Sternwarte Bonn 59, 48
Ayani K., 2015, IAUC, 9279, 3
Ayani K., Maeno S., 2014, CBET, 3841, 1
Banerjee D. P. K., Ashok N. M., 2012, BASI, 40, 243
Belczyński K., Mikołajewska J., Munari U., Ivison R. J., Friedjung M., 2000, A&AS, 146, 407
Bessell M. S., 1990, PASP, 102, 1181
Bode M. F., Evans A. eds, 2012, Classical Novae. Cambridge Univ. Press, Cambridge
Buscombe W., de Vaucouleurs G., 1955, Obs, 75, 170
Campbell H. et al., 2015, ATel, 8155
Capaccioli M., della Valle M., Rosino L., D'Onofrio M., 1989, AJ, 97, 1622
Chomiuk L. et al., 2014, Nature, 514, 339
Chomiuk L., Strader J., Stanek K. Z., Kochanek C. S., Holoien T. W.-S., Shappee B. J., Prieto J. L., Dong S., 2016, ATel, 8841
Cousins A. W. J., 1980, South African Astronomical Observatory Circular, 1, 166
Darnley M. J. et al., 2004, MNRAS, 353, 571
Darnley M. J. et al., 2006, MNRAS, 369, 257
Downes R. A., Duerbeck H. W., 2000, AJ, 120, 2007
Duerbeck H. W., 2008, in Bode M.-F., Evans A., eds, Classical Novae. Cambridge Univ. Press, Cambridge, p 1
Fiorucci M., Munari U., 2003, A&A, 401, 781
Fitzpatrick E. L., 1999, PASP, 111, 63
Fluks M. A., Plez B., The P. S., de Winter D., Westerlund B. E., Steenman H. C., 1994, A&AS, 105, 311
Frank S., Wagner R. M., Starrfield S., Woodward C. E., Neric M., 2016, ATel, 8817
Graham J. A., 1982, PASP, 94, 244
Henden A., Munari U., 2008, Baltic Astron., 17, 293
Henden A., Munari U., 2014, in Pribulla T., ed., Observing Techniques, Instrumentation and Science for Meter-Class Telescopes, CoSka, 43, 518
Henden A. A., Levine S. E., Terrell D., Smith T. C., Welch D., 2012, Journal of the American Association of Variable Star Observers, 40, 430
Hjellming R. M., 1974, in Verschuur G. L., Kellermann K. I., eds, Galactic and Extra-Galactic Radio Astronomy. Springer, New York, p. 159
Hounsell R. et al., 2010, ApJ, 724, 480
Jablonski F., Oliveira A., 2016, ATel, 9684
Jelinek M., Cunniffe R., Castro-Tirado A. J., Rabaza O., Hudec R., 2014, ATel, 6025
Johnson H. L., Morgan W. W., 1953, ApJ, 117, 313
Joshi V., Banerjee D. P. K., Venkataraman V., Ashok N. M., 2014, ATel, 6032
Joshi V., Banerjee D. P. K., Ashok N. M., Venkataraman V., Walter F. M., 2015, MNRAS, 452, 3696
Kasliwal M. M., Cenko S. B., Kulkarni S. R., Ofek E. O., Quimby R., Rau A., 2011, ApJ, 735, 94 (K11)
Koornneef J., 1983, A&A, 128, 84
Krautter J., 2008, in Evans A., Bode M. F., O'Brien T. J., Darnley M. J., eds, ASP Conf. Ser. Vol. 401, RS Ophiuchi (2006) and the Recurrent Nova Phenomenon. Astron. Soc. Pac., San Francisco, p. 139
Kuin N. P. M., Page K. L., Williams S. C., Darnley M. J., Shore S. N., Walter F. M., 2016, ATel, 9635
Kuulkers E., Page K. L., Saxton R. D., Ness J.-U., Kuin N. P., Osborne J. P., 2014, ATel, 6015
Landolt A. U., 1992, AJ, 104, 340
Landolt A. U., 2009, AJ, 137, 4186
Li K-L., Chomiuk L., 2016, ATel, 9699
Li K-L., Chomiuk L., Strader J., 2016a, ATel, 9736
Fermi Large Area Telescope CollaborationLi K-L., Chomiuk L., Strader J., Cheung C. C., Jean P., Shore S. N., 2016b, ATel, 9771
Linford J. et al., 2015, ATel, 7194
Linford J. D. et al., 2017, preprint (arXiv:1703.03333)
Lipunov V. et al., 2016, ATel, 9631
Littlefield C., Garnavich P., 2015, ATel, 8156
Luckas P., 2016, ATel, 9678
Lukas P., 2016, ATel, 9658
McLaughlin D. B., 1960, in Greenstein J. L., ed., Stellar Atmospheres. University of Chicago Press, Chicago, p. 585
Mateo M. L., 1998, ARA&A, 36, 435
Mezger P. G., Henderson A. P., 1967, ApJ, 147, 471
Morris P. J., Cotter G., Brown A. M., Chadwick P. M., 2017, MNRAS, 465, 1218
Mróz P., Udalski A., 2016a, ATel, 8811
Mróz P., Udalski A., 2016b, ATel, 9622
Mróz P. et al., 2015, ApJS, 219, 26
Mróz P., Udalski A., Pietrukowicz P., 2016a, ATel, 9683
Mróz P. et al., 2016b, ApJS, 222, 9
Munari U., 2014, in Woudt P. A., Ribeiro V. A. R. M., eds, ASP Conf. Ser. Vol. 490, Stella Novae: Past and Future Decades. Astron. Soc. Pac., San Francisco, p. 183
Munari U., Moretti S., 2012, Baltic Astron., 21, 22
Munari U., Yudin B. F., Taranova O. G., Massone G., Marang F., Roberts G., Winkler H., Whitelock P. A., 1992, A&AS, 93, 383
Munari U. et al., 2011, MNRAS, 410, L52
Munari U. et al., 2012, Baltic Astron., 21, 13

Munari U., Dallaporta S., Castellani F., Valisa P., Frigo A., Chomiuk L., Ribeiro V. A. R. M., 2013, MNRAS, 435, 771
Munari U., Henden A., Frigo A., Dallaporta S., 2014a, Journal of Astronomical Data, 20, 4
Munari U. et al., 2014b, AJ, 148, 81
Munari U., Maitan A., Moretti S., Tomaselli S., 2015, New Astron., 40, 28
Munari U., Walter F. M., Hambsch F.-J., Frigo A., 2016a, IBVS, 6162, 1
Munari U., Sollecchia U., Hambsch F.-J., Frigo A., 2016b, IAUC, 9280
Muneer S., Anupama G. C., 2016, ATel, 8853
Muneer S., Anupama G. C., Raveendran A. V., 2015, ATel, 7161
Nelson T., Mukai K., Sokoloski J., Chomiuk L., Rupen M., Mioduszewski A., Page K., Osborne J., 2012, ATel, 4590
Nelson T. et al., 2015, ATel, 7085
Ness J. U., 2012, Bulletin of the Astronomical Society of India, 40, 353
Orio M., Behar E., Rauch T., Zemk P., 2016a, ATel, 9810
Orio M., Rauch T., Zemko P., Behar E., 2016b, ATel, 9970
Osborne J. P. et al., 2010, ATel, 2442
Özdönmez A., Güver T., Cabrera-Lavers A., Ak T., 2016, MNRAS, 461, 1177
Page K. L. et al., 2013, ATel, 4845
Page K. L., Osborne J. P., Kuulkers E., 2014, ATel, 6035
Page K., Osborne J., Kuin P., Shore S., Williams S., Darnley M. J., 2016, ATel, 9733
Rudy R. J., Crawford K. B., Russell R. W., 2016, ATel, 9849
Saikia D. J., Anupama G. C., 2012, eds. Novae from Radio to Gamma-rays, BASI 40
Saito R. K., Minniti D., Catelan M., Angeloni R., 2016, ATel, 9680
Schlafly E. F., Finkbeiner D. P., 2011, ApJ, 737, 103 (SF11)
Schlegel D. J., Finkbeiner D. P., Davis M., 1998, ApJ, 500, 525 (SFD98)
Schwarz G. J. et al., 2011, ApJS, 197, 31
Seitter W. C., 1990, in Cassatella A., Viotti R., eds, Physics of Classical Novae. Springer, Berlin, p. 79
Shara M. M. et al., 2017, ApJ, 839, 109
Shumkov V. et al., 2016, ATel, 9621
Smith J. A. et al., 2002, AJ, 123, 2121
Sowell J. R., Trippe M., Caballero-Nieves S. M., Houk N., 2007, AJ, 134, 1089
Srivastava M., Ashok N. M., Banerjee D. P. K., Venkataraman V., 2015a, ATel, 7236
Srivastava M. K., Ashok N. M., Banerjee D. P. K., Sand D., 2015b, MNRAS, 454, 1297
Srivastava M., Joshi V., Banerjee D. P. K., Ashok N. M., 2016, ATel, 8809
Stanek K. Z. et al., 2016, ATel, 9669
Straižys V., 1992, Multicolor Stellar Photometry. Pachart Publishing House, Tucson
van den Bergh S., Younger P. F., 1987, A&AS, 70, 125
Walter F., 2015, ATel, 7060
Walter F. M., Battisti A., Towers S. E., Bond H. E., Stringfellow G. S., 2012, PASP, 124, 1057
Warner B., 1995, Cataclysmic Variable Stars. Cambridge Univ. Press, Cambridge
Weston J. H. S. et al., 2016, MNRAS, 457, 887
Williams R. E., 1992, AJ, 104, 725
Williams S. C., Darnley M. J., 2016a, ATel, 9628
Williams S. C., Darnley M. J., 2016b, ATel, 9688
Woudt P. A., Ribeiro V. A. R. M. eds, 2014, ASP Conf. Ser. Vol. 490, Stella Novae: Past and Future Decades. Astron. Soc. Pac., San Francisco

SUPPORTING INFORMATION

Supplementary data are available at *MNRAS* online.

Table 2. Our BVI_C photometry of the programme novae.

Please note: Oxford University Press is not responsible for the content or functionality of any supporting materials supplied by the authors. Any queries (other than missing material) should be directed to the corresponding author for the article.

This paper has been typeset from a TEX/LATEX file prepared by the author.